物理化学学报(*Wuli Huaxue Xuebao*)
2404 *Acta Phys. -Chim. Sin.* **2017,** *33* (12), 2404−2423 December

[Review] doi: 10.3866/PKU.WHXB201706263 www.whxb.pku.edu.cn

石墨烯基复合材料应用于光电二氧化碳还原的基本原理, 研究进展和发展前景

全 泉[1] 谢顺吉[2] 王 野[2,*] 徐艺军[1,*]

([1]福州大学化学学院，能源与环境光催化国家重点实验室，福州 350116；
[2]厦门大学化学化工学院，固体表面物理化学国家重点实验室，能源材料化学协同创新中心，福建 厦门 361005)

摘要 :面对日益严重的化石能源消耗和温室效应问题, 二氧化碳还原正成为一个重要的全球性研究课题, 其通过消耗二氧化碳来生成可用于能源供应的产物。光电催化技术同时利用光能和外部电压，是一种用于二氧化碳还原的可行且有效的途径。因为石墨烯具有增强二氧化碳吸附和促进光生电子转移的特性能够提升石墨烯基复合电极的性能，所以引入石墨烯用于调优光电催化二氧化碳还原体系已经引起了广泛关注。本篇综述详细陈述了石墨烯基复合材料应用于光电二氧化碳还原的基本原理，电极制备方法以及目前的研究进展。我们也对这个蓬勃发展的领域未来可能会遇到的机遇和挑战进行了展望，同时提出了潜在可行的革新策略用于提升光电二氧化碳还原方面的研究。

关键词：光电催化；二氧化碳还原；石墨烯基复合材料
中图分类号：O649

Photoelectrochemical Reduction of CO_2 over Graphene-Based Composites: Basic Principle, Recent Progress, and Future Perspective

QUAN Quan[1] XIE Shun-Ji[2] WANG Ye[2,*] XU Yi-Jun[1,*]

([1]*State Key Laboratory of Photocatalysis on Energy and Environment, College of Chemistry, Fuzhou University, Fuzhou 350116, P. R. China;* [2]*State Key Laboratory of Physical Chemistry of Solid Surfaces, Collaborative Innovation Center of Chemistry for Energy Materials, College of Chemistry and Chemical Engineering, Xiamen University, Xiamen 361005, Fujian Province, P. R. China*)

Abstract: In response to aggravated fossil resources consuming and greenhouse effect, CO_2 reduction has become a globally important scientific issue because this method can be used to produce value-added feedstock for application in alternative energy supply. Photoelectrocatalysis, achieved by combining optical energy and external electrical bias, is a feasible and promising system for CO_2 reduction. In particular, applying graphene in tuning photoelectrochemical CO_2 reduction has aroused considerable attention because graphene is advantageous for enhancing CO_2 adsorption, facilitating

Received: June 5, 2017; Revised: June 19, 2017; Published online: June 26, 2017.
*Corresponding authors. WANG Ye, Email: wangye@xmu.edu.cn. XU Yi-Jun, Email: yjxu@fzu.edu.cn.
The project was supported by the National Natural Science Foundation of China (U1463204, 20903023 and 21173045), the Award Program for Minjiang Scholar Professorship, the Natural Science Foundation of Fujian Province for Distinguished Young Investigator Grant (2012J06003), the Independent Research Project of State Key Laboratory of Photocatalysis on Energy and Environment (2014A05), the first Program of Fujian Province for Top Creative Young Talents, the Open Research Project of State Key Laboratory of Physical Chemistry of Solid Surfaces of Xiamen University (201519), the Program for Returned High-Level Overseas Chinese Scholars of Fujian province, and the Natural Science Foundation of Fujian Province for Distinguished Young Investigator Rolling Grant (2017J07002).
国家自然科学基金(U1463204, 20903023 和 21173045)，闽江学者特聘教授科研启动基金，福建省杰出青年自然科学基金(2012J06003)，能源与环境光催化国家重点实验室自主课题(2014A05)，福建省首批特支人才“双百计划”青年拔尖创新人才，厦门大学固体表面物理化学国家重点实验室开放课题(201519)，教育部留学回国人员科研启动基金项目，福建省杰出青年自然科学基金滚动资助项目(2017J07002)

electrons transfer, and thus optimizing the performance of graphene-based composite electrodes. In this review, we elaborate the fundamental principle, basic preparation methods, and recent progress in developing a variety of graphene-based composite electrodes for photoelectrochemical reduction of CO_2 into solar fuels and chemicals. We also present a perspective on the opportunities and challenges for future research in this booming area and highlight the potential evolution strategies for advancing the research on photoelectrochemical CO_2 reduction.

Key Words: Photoelectrochemical; CO_2 reduction; Graphene-based composite

1 Introduction

With human society developed rapidly, the depletion of fossil resources and the deterioration of greenhouse effect have become global issues[1,2]. CO_2 as one of key components of greenhouse gas is potential to be utilized producing solar fuels[3–6]. Therefore, the demand for the future energy supply and global environment improvement has stimulated research activities towards the efficient reduction of CO_2 to value added products. However, because CO_2 is a stable molecule with high thermodynamic stability and kinetic inertness, the reduction of CO_2 is required to break a high activation barrier and regarded as a challenging research theme in chemical science[7,8].

The plants photosynthesis, an important medium for nature carbon cycle, is to transform CO_2 with H_2O into carbohydrates and O_2 under sunlight illumination at room temperature. Enlightened by this natural process, numerous research efforts have been devoted to developing artificial or synthetic photocatalysts for converting CO_2 into useful chemicals

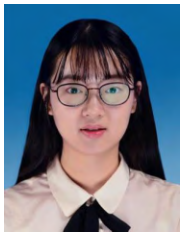

QUAN Quan is now pursuing her PhD degree under the supervision of Prof. XU Yi-Jun at the State Key Laboratory of Photocatalysis on Energy and Environment, College of Chemistry, Fuzhou University, P. R. China. Her current research interests include composite materials synthesis and their applications in energy conversion and storage such as photocatalytic and photoelectrochemical redox processes.

WANG Ye obtained his PhD degree in 1996 from Tokyo Institute of Technology. He then worked at Tokyo Institute of Technology, Tohoku University and Hiroshima University during 1996–2000. He was promoted to associate professor at Hiroshima University in 2001. He became a professor of Xiamen University in the August of 2001. He is currently the director of State Key Laboratory of Physical Chemistry of Solid Surfaces and the director of Institute of Catalysis Science and Technology of Xiamen University. The group of Professor Wang works on catalysis for efficient utilization of carbon resources including the selective transformation of methane, syngas, biomass and CO_2 into fuels and chemicals.

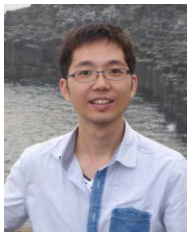

XIE Shun-Ji received his BS and MSc degrees from Hunan University of China in 2008 and 2011, and obtained his PhD degree from Xiamen University in 2014. He is currently an iChEM Fellow in the Collaborative Innovation Center of Chemistry for Energy Materials, Xiamen University, China. He focuses on photocatalytic energy conversion, especially CO_2 reduction.

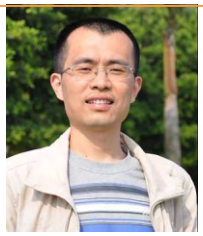

XU Yi-Jun received his PhD degree in heterogeneous catalysis at School of Chemistry, Cardiff University, U.K. in 2006 with the supervision of Prof. Graham J. Hutchings (FLSW FRS). From 2007 to 2009, he worked as a postdoctoral fellow at the Fritz-Haber Institute of the Max Planck Society, Berlin, Germany. After that, he became a full professor working at State Key Laboratory of Photocatalysis on Energy and Environment, College of Chemistry, Fuzhou University, P.R. China. He is a Fellow of Royal Society of Chemistry (FRSC) and his current research interests primarily focus on the assembly and applications of composite materials, such as graphene-based semiconductor composites, core-shell composites and metal-based nanostructured materials, in the field of heterogeneous photocatalysis.

including carbonic oxide, formic acid, formaldehyde, methanol, ethanol, methane, higher hydrocarbons, etc.[9–14]. While multitudinous encouraging achievements have been gained toward artificial photocatalytic reduction of CO_2, further effort is still required to increase the solar-to-fuel efficiencies, promote the selectivity of products and reinforce the stability of photocatalysts[13,15]. Besides, the electrochemical CO_2 reduction is another significant route for the transformation of CO_2 to value added feedstocks[16]. Because the electrochemical devices are not limited by traditional thermochemical cycles, their achievable efficiency is often significantly higher than their chemical counterpart. Meanwhile, the separated non-direct reactions permit researchers to tailor the properties needed for each redox process independently[17]. However, generally a high overpotential for electrocatalysis is needed to overcome the energy barrier of CO_2 reduction[18]. At standard pressure, the solubility of CO_2 in aqueous solution is low. Thus, higher pressures are necessary to increase the CO_2 concentration in the liquid phase, which, in turn, limit the electrode stability[19].

Nowadays, with combination of heterogeneous photocatalysis and electrochemical techniques, photoelectrocatalysis is regarded as an alternative and powerful approach for CO_2 reduction[20]. On one hand, introducing solar energy can markedly lower the applied voltage in comparison with the electrocatalysis. On the other hand, the imposition of an external electrical bias can facilitate the separation of electrons and holes, which is of significant importance to promote the photocatalytic efficiency. Furthermore, the photoelectrochemical, physically separating the stages of oxidation and reduction in dual-chamber, can avoid the re-oxidation of obtained products as well as other negative reacting competitions[21]. In 1978, Halmann *et al.*[22] earliest reported the photoelectrocatalytic reduction of CO_2, using *p*-type gallium phosphide as a photocathode to reduce aqueous carbon dioxide, getting formic acid, formaldehyde and methanol as products. Henceforth, this research direction has been extensively studied.

In fact, just in regard to an experimental setup, photoelectrochemical reaction is similar to electrochemical reaction[23]. Instead of conductor electrodes applied in electrochemistry, photoelectrochemical devices use semiconductor as one or two electrodes to be light harvester. When activity at semiconductor surface for CO_2 reduction is poor, the corresponding photoelectrocatalytic reaction rate is definitely slow, irrespective of a level of applied external potential. Therefore, selecting the appropriate electrode materials and optimizing their performance are significantly crucial for realizing the high-efficiency of photoelectrocatalytic reaction. In recent years, graphene has rocketed as a shining star material, which not only is now available at large quantities, but also possesses many unique properties such as high surface area, excellent conductivity and mechanical strength[24,25]. Therefore, many research efforts have been paid to combine graphene with semiconductors as synergistic heterogeneous composites to improve the efficiency of either photocatalytic or electrochemical CO_2 reduction[25–28]. Notably, graphene and graphene-based composites have also stepped into the photoelectrochemical fields and been applied to optimize the composition and the performance of photoelectrodes[29–31].

The goal of this review is to describe the current status of the use of graphene in tuning the efficiency of photoelectrochemical CO_2 reduction to solar fuels and chemicals over graphene-based composites, and demonstrate how to prepare graphene-based composite electrodes and utilize the key property of graphene to facilitate photoelectrochemical reduction of CO_2 by selecting typical examples in this research field. Beyond that, we will discuss the potential strategies that can be evolved to optimize the performance of photoelectrochemical CO_2 reduction, the possible opportunities and key challenges in future development of this research area.

2 Basic principle of photoelectrochemical CO_2 reduction over graphene-based composites

When CO_2 reduction is conducted in the cathodic chamber of photoelectrochemical cell, the H_2O oxidation is typically adopted as electron donor and proton source in the anodic chamber[32,33], which has been reported in many researches and reviews[9,10,21,34–40]. Therefore, the coupling of CO_2 reduction with H_2O oxidation to form closing of the complete photoelectrochemical cycle is the premise of following elaboration.

2.1 Thermodynamics and pathways of CO_2 reduction

Photoelectrochemistry is regarded as a multidisciplinary field involving photochemistry, electrochemistry, surface science and solid-state physics[41]. Before discussion about the rationales of photoelectrochemical reduction of CO_2, the thermodynamics of CO_2 reduction and the pathways of CO_2 electroreduction are first elaborated to provide a preliminary comprehension. Because of high stability of linear structure and low energy grade of CO_2 molecule, the chemical transformations of CO_2 are thermodynamically highly unfavorable[42]. The standard Gibbs free energies (ΔG^0) and the standard redox potential (ΔE^0) of the multi-electron CO_2 reduction are listed in Table 1. Obviously, the ΔG^0 values of the reduction of CO_2 with water are all highly positive, indicating that a large input of external energy is required to drive the desired transformations. Therefore, the reaction of CO_2 reduction is quite challenging.

So far, various hypothesizes concerning mechanism of CO_2 reduction have been explored and proposed by different research groups[43–48], which are indicated as complex multistep reactions involving shared intermediates and multiple reaction pathways. The electron paramagnetic resonance (EPR) spectroscopy, *in situ* diffuse reflectance infrared Fourier transform spectroscopy (DRIFTS), transient absorption

Table 1 Thermodynamics of CO_2 reduction.

Reaction	Production	Transferred electron numbers	ΔG^0/(kJ·mol^{-1})	ΔE^0/V
$CO_2(g) \rightarrow CO(g) + 1/2O_2(g)$	CO	2	257	1.33
$CO_2(g) + H_2O(l) \rightarrow HCOOH(l) + 1/2O_2(g)$	HCOOH	2	286	1.48
$CO_2(g) + H_2O(l) \rightarrow HCHO(l) + O_2(g)$	HCHO	4	522	1.35
$CO_2(g) + 2H_2O(l) \rightarrow CH_3OH(l) + 3/2O_2(g)$	CH_3OH	6	703	1.21
$CO_2(g) + 2H_2O(l) \rightarrow CH_4(g) + 2O_2(g)$	CH_4	8	818	1.06
$CO_2(g) + 3/2H_2O(l) \rightarrow 1/2C_2H_5OH(l) + 3/2O_2(g)$	C_2H_5OH	6	663	1.14
$CO_2(g) + H_2O(l) \rightarrow 1/2C_2H_4(g) + 3/2O_2(g)$	C_2H_4	6	666	1.15
$CO_2(g) + 3/2H_2O(l) \rightarrow 1/2C_2H_6(g) + 7/4O_2(g)$	C_2H_6	7	734	1.09

spectroscopy (TAS) and scanning tunneling microscope (STM) are employed as exploratory techniques to investigate the reaction mechanism and pathways[49]. The typical two-electron reduced reaction pathways for electroreduction of CO_2 in aqueous medium are illustrated in Fig.1A. The initial step is that CO_2 molecule accepts one electron to form the carbon dioxide anion radical ($CO_2^{\bullet-}$)[50], which is more likely to be broken due to the bending structure in contrast to linear geometry structure of CO_2 [51]. When $CO_2^{\bullet-}$ is adsorbed on the electrode, H^+ in aqueous media may easily react with the O atom, because C atom is bonded to the surface preventing reaction with H^+ [50]. The CO_2H(ads), formed in this way, will be further reduced by another electron into adsorbed CO, or may participate in subsequent complex reaction with H^+ and electrons turning into CH_4, CH_3OH or other value-added hydrocarbons[52]. When $CO_2^{\bullet-}$ is not adsorbed on the electrode in aqueous solution, the nucleophilic carbon atom acts as the Lewis base and the formate ion is formed with intrusion of second electron. Interestingly, CO_2 molecule contains delocalized π-conjugated binding, while graphene manifests a large 2D π-conjugated structure, which results in a strong π–π conjugation interaction established between graphene and CO_2 molecule (Fig.1B). The reaction intermediates such as $CO_2^{\bullet-}$ with a delocalized electronic structure can also be attached onto graphene through π–π non-covalent bonds[53]. When graphene-based composites act as electrodes for CO_2 reduction, the strong π–π conjugation can facilitate CO_2 adsorption and also contribute to the destabilization and activation of CO_2 molecules[54,55]. Moreover, the theoretical surface area of a single graphene sheet is 2630 m^2·g^{-1} [56], providing a large number of adsorption sites for the CO_2 molecules. Therefore, the large surface area and strong π–π conjugation provide synergistic effects on promoting CO_2 adsorption, thus resulting in tuning the efficiency of reaction for CO_2 reduction.

The process of CO_2 reduction is highly sensitive to the reaction conditions, such as pH, external bias, electrode surface structure, temperature, pressure and so on[57]. Thereinto, the pH value of the electrolyte has critical impact on the preferred reaction pathway and the final products. At a low pH value, the competing hydrogen evolution reaction (HER) dominates while the reaction rates for CO_2 reduction improve with the increase in pH values. The external bias on the cathode plays an

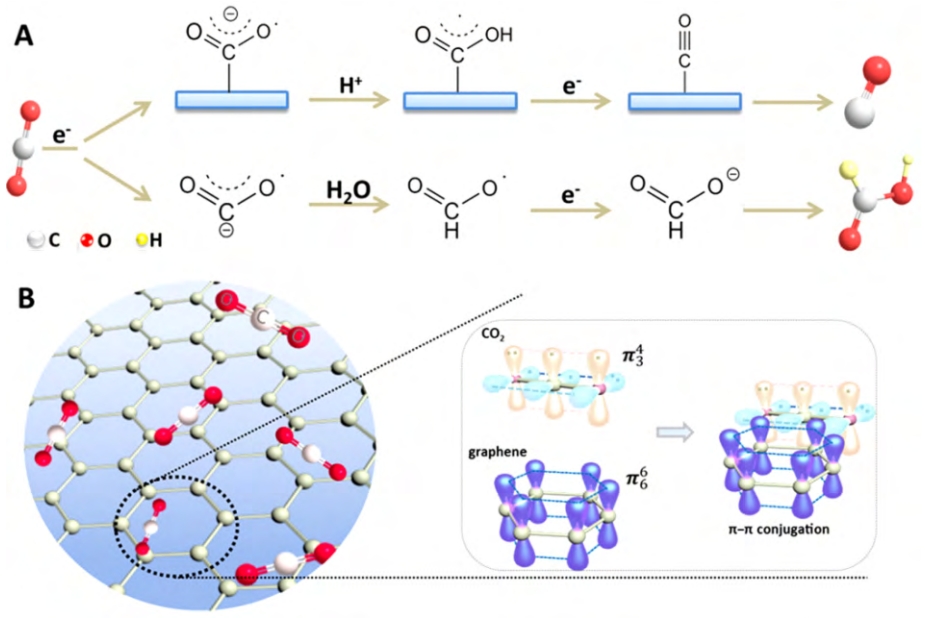

Fig.1 (A) Two-electron reaction mechanism of CO_2 reduction in aqueous solutions, (B) The formation of π-π conjugation interaction between graphene and CO_2 molecule.

important role in the product distribution of CO_2 reduction. Furthermore, the negative external bias should be controlled applicably in order to avoid the competitive HER and promote CO_2 conversion. As for graphene-based composites, different weight ratio of graphene could also influence the selectivity of products for CO_2 reduction. For instance, Han *et al.*[53] have found that with the increase of the weight ratio of graphene in the graphene-TiO_2 composites, the production rate of CH_4 slowly decreases while the production rate of C_2H_6 increases to some degree. Actually, the pathway of CO_2 reduction is more complicated in specific reaction than the aforementioned theories depending on the practical conditions. The conclusive evidence about the reaction mechanism for CO_2 reaction is still not available[42,52], so that the pathways of CO_2 reduction and the mechanism of graphene-based composites for CO_2 reduction need further exploration.

2.2 Categories and processes of photoelectrochemical CO_2 reduction

A photoelectrochemical setup typically contains four components. Firstly, the electrolyte is an essential component. The common used electrolytes for photoelectrochemical reduction of CO_2 include carbonates, sulfates, phosphates, perchlorates of alkali salts, and tetraalkylammonium salts, etc., all of which can affect the distribution of products by influencing the reaction pathways. Generally, the carbonates favor formic acid production while the other electrolytes favor the formation of carbon monoxide[58]. Secondly, the conductive substrate is a basic component. Traditionally, it is fluorine doped tin oxide (FTO) or indium tin oxide (ITO) glass. Nowadays, metal foil (e.g., Cu foil[59], Ti foil[60]) and metal foam (e.g., Ni foam[61], Cu foam[62]) are also developed as substrates. Thirdly, the semiconductor film anchored on substrate as working electrode is the most important component for the efficiency of photoelectrochemical setup. Fourthly, a counter electrode (e.g., platinum electrode) is applied to conduct the half reaction cooperating with working electrode to form the complete photoelectrochemical cycle. There are other components applied in a photoelectrochemical setup depending on specific demand. For example, the reference electrode (RE) (e.g., Ag/AgCl electrode, saturated calomel electrode) is used in the three-electrode system and the proton exchange membrane is needed in a dual-chamber system to delivery proton (H^+). In contrast, the two-electrode and single-chamber photoelectrochemical setups do not employ reference electrodes and proton exchange membranes, respectively.

As for the semiconductor film in the photoelectrochemical system, it generates electron-hole pairs after absorbing equal or higher photon energy than its intrinsic band gap energy (E_g). Depending on the charge densities of electrons and holes, semiconductors can be typically categorized into two types. Simply speaking, semiconductors providing electrons as the majority charge carrier are defined as *n*-type semiconductors, while *p*-type semiconductors use positively charged holes as the majority charge carrier[63]. When *n*-type or *p*-type semiconductors are placed into an electrolyte solution, if the Fermi level (E_F) of a semiconductor does not match the redox potential (E_R) of the electrolyte, a charge transfer between the semiconductor and liquid phase will take place and thus a band bending will be induced to render changed E_F matching the E_R[64,65]. Specifically, as for a *p*-type semiconductor, the E_F is located above the valence band but below the E_R. The interfacial electrons flow towards the semiconductor to attain equilibrium, resulting in an increase in the Fermi level energy to match the E_R. Thus, a downward band bending is established, which facilitates conduction band electrons moving to semiconductor-electrolyte (S-E) interface[66], as depicted in Fig.2A. Conversely, the *n*-type semiconductor occurs an upward band bending that moves valence band holes toward the S-E interface (Fig.2B). Therefore, *p*-type semiconductors are generally used in the reduction compartment as photocathodes because the electrons can flow toward the S-E interface to accelerate the CO_2 reduction. The anodic chamber usually utilizes *n*-type semiconductors considering that upward band bending enables holes to shift toward the S-E interface facilitating the H_2O oxidation.

Generally, the photoelectrochemical setups can be classified into three typical types: (I) the *p*-type semiconductors as photocathodes with counter electrodes; (II) the *n*-type semiconductors as photoanodes with counter electrodes. The type III is a peculiar category combining the *p*-type

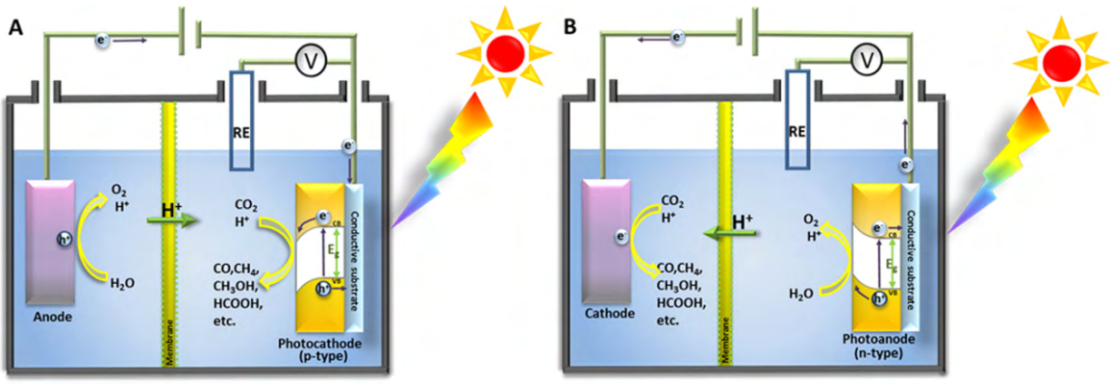

Fig.2 Schematic illustrations of (A) type I and (B) type II for photoelectrochemical setup.

semiconductors as photocathodes and *n*-type semiconductors as photoanodes, whose working mechanism is same to type I and type II and will be discussed in Section 5.1. Fig.2(A, B) respectively illustrate the type I and type II in a three-electrode dual-chamber photoelectrochemical setup, in which type I is taken as an example to elaborate the process and mechanism of photoelectrochemical CO_2 reduction. The *p*-type semiconductor adsorbs photons under light illumination to create electron-hole pairs, with the conductive band electrons moving to the S-E interface and the holes migrating toward conductive substrate. The external circuit is conducted by a potentiostat (i.e., electron pump)[67], which drives electrons flow to the photocathode and then deplete with the generated holes on the cathode. This process efficiently suppresses the recombination of electrons and holes on the semiconductor. The counter electrode remains holes reacting with H_2O into O_2 and H^+. The H^+ is transmitted from anolyte to catholyte by membrane and then cooperates with electrons at the S-E interface to react with CO_2 into CO, CH_4, CH_3OH, HCOOH, etc. Under cooperation with light illumination and external bias, the complete photoelectrochemical cycle with CO_2 reduction and H_2O oxidation can keep continuous running.

Viewing the elaboration for the whole process of photoelectrochemical CO_2 reduction, minimizing electron-hole pairs recombination and accelerating electrons transfer are significantly pivotal for enhancing photoelectrochemical activity[68]. Because of their good electrical conductivity coupled with a large interface area, carbon materials are often the desirable choice of the electrode. Furthermore, graphene is an excellent candidate for optimizing the electron transfer when acting as electrode materials[69,70]. In photocatalysis fields, the most-widely recognized role of graphene is an electron reservoir to accept, transport, and shuttle electrons photogenerated from the excitation of photoactive components in the composites[71,72]. The electrons rapidly transfer from the photoactive catalyst to graphene while photoinduced holes remain in the photocatalyst, which contributes to suppressing electron-hole pairs recombination[73,74]. Therefore, in the photoelectrochemical system, graphene can have a synergetic effect with external bias, which could further facilitate electron transfer and suppress the electron-hole pairs recombination. More interestingly, graphene can alter the conduction band potential of semiconductor to form graphene-based composite, which induces the occurrence of reduction of CO_2 [75]. Bai *et al.*[76] have reported that graphene/WO_3 nanobelt composites are able to reduce CO_2 into CH_4, in which graphene elevates the conduction band of WO_3 in the composites while the single WO_3 is inherently limited to reduce CO_2. On the other hand, it is should be noted that when a graphene-based composite is applied for CO_2 reduction, the carbonaceous products are possible to be obtained from the hydrogenation of the acid and alcoholic groups on graphene to lower the veracity of results. For dispelling the suspicion, relevant test experiments are necessary to confirm the original sources of products. For example, the experiment in the inert gases (e.g., N_2, Ar) rather than CO_2 atmosphere could be conducted under same condition to detect the product[77]. Besides, the more precise method is to conduct an isotope tracing experiment, for example, isotope tracing experiment using $^{13}CO_2$ gas[78].

3 Fabrication of graphene-based composite electrodes

The preparation methods of (photo)electrodes on substrates can remarkably influence the physicochemical properties of assembled electrodes (e.g., thickness, homogeneity)[79] and thus affect their photoelectrochemical performances. It is crucial to utilize suitable preparation methods of electrodes for constructing high-performance photoelectrochemical system. The basic methods of (photo)electrodes preparation includes dip-coating, drop-casting, spray-coating, spin-coating, electrostatic layer-by-layer self-assembly, electrodeposition and electrophoretic deposition, etc.[79–82]. As for graphene-based composite electrodes, the conventional fabrication methods are chemical vapor deposition (CVD) of graphene sheets on substrates with finely tuned temperature and pressure conditions[83,84], or electrophoretic and electrodeposition of graphene or its precursor (e.g., graphene oxide) onto target films[71]. The other general methods can also be applied to prepared graphene and graphene-based composites on substrates as electrodes for desirable applications. There are many reviews focusing on the synthetic methods for graphene and its derivatives but rarely paying attention to the preparation methods for graphene or graphene-based electrodes[85–88]. Therefore, we will summarize and elaborate the basic preparation methods for graphene or graphene-based composites on target substrates as (photo)electrodes in this section.

3.1 Physical coating methods

The physical preparation methods are to adhere available graphene or graphene-based composites on target substrates without varying their physicochemical properties. The dip-coating and drop-casting are two of the simplest approaches to conduct because of their easily available apparatus and mild operation conditions. Generally, the target material suspension is deposited onto the substrate surface by a dropping or dip-lift method and then dried for evaporation of solvents, leaving the composite films formed on the substrate[72], as illustrated in Fig.3(A, C), respectively. For instance, Amal *et al.*[89] have drop-casted ethanol solution containing $BiVO_4$-reduced graphene oxide ($BiVO_4$-RGO) composites on the FTO electrodes with the aid of a micro-syringe and then dried the electrodes under flowing air for evaporation of the ethanol, leaving the $BiVO_4$-RGO homogeneously deposited on FTO surface (Fig.3B). Because single dip-coating method has some inevitable problems, e.g., the nonuniform coverage and the weak interfacial contact between materials and substrates,

the strategies combining dip-coating and electrostatic layer-by-layer self-assembly are usually applied to fabricate desirable graphene-based composites electrodes[90,91]. As a typical example, Liu *et al.*[28] have fabricated RGO-CdS quantum dots (QDs) composites on FTO substrate. Firstly, the cleaned FTO substrate is rapidly dipped into poly(diallyldimethylammoniumchloride) (PDDA) aqueous solution to have a positively charged surface; Secondly, the FTO is immersed in negatively charged CdS QDs aqueous solution; Finally, the resultant substrate is dipped into positively charged RGO-poly(allylamine hydrochloride) (PAH) aqueous solution. The multilayered films with desired film thickness can be fabricated by repeating the number of dipping cycles (Fig.3D).

Besides, the spin-coating method is also an alternative for fabricating graphene or graphene-based composite electrodes. A small amount of coating material is put on the center of the substrate and then rotated at high speed to spread the coating material by centrifugal force. After drying, the film material is formed (Fig.4A). The spin coating speeds can vary the orientation of the graphene sheets in the composite thin films. Chhowalla *et al.*[92] have found that at high spin-coating speeds (2000 r·min^{-1}), the graphene sheets are sparsely distributed and oriented almost parallel to the substrate surface (Fig.4B). At lower spin-coating speeds (600 r·min^{-1}), graphene sheets are densely distributed over the substrate (Fig.4C). The shear force is small thus to form the random orientation of graphene sheets. Jang *et al.*[93] have fabricated graphene oxide/hematite (GO/α-Fe_2O_3) photoanode on FTO, in which GO is coated by spin-coating and serves as a sacrificial underlayer. They have also discovered that varying the spin speed from 3000 to 6000 r·min^{-1} leads to an improved photocurrent (30% increase) from 1 to 1.3 mA·cm^{-2} at 1.4 V *vs.* reversible hydrogen electrode

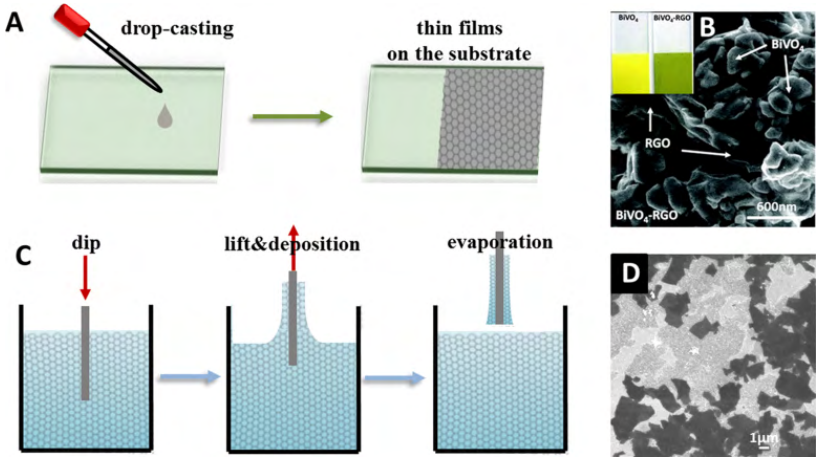

Fig.3 (A) Schematic illustration of a drop-casting process, (B) SEM image of $BiVO_4$-RGO (the inset is photographs of $BiVO_4$ and $BiVO_4$-RGO electrodes), (C) Schematic illustration of a dip-coating process, (D) FESEM image of RGO-CdS QDs composite films self-assembled on FTO substrate with the same five deposition cycles.

(B) is reprinted with permission from Ref.89, Copyright 2010 American Chemical Society. (D) is reprinted with permission from Ref.28, Copyright 2010 American Chemical Society.

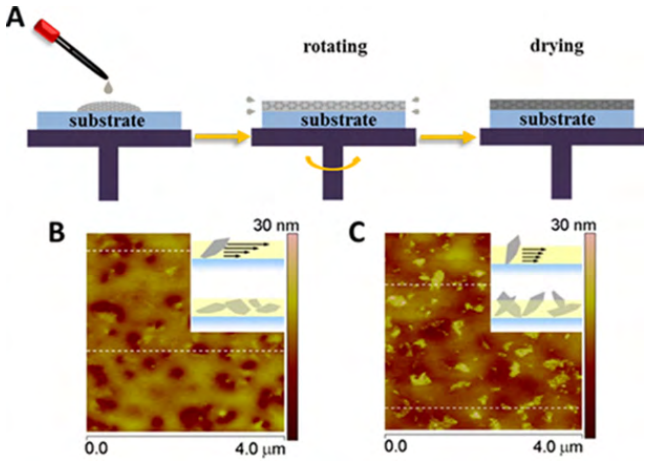

Fig.4 (A) Schematic illustration of a spin-coating process, (B) AFM image of thin films prepared at 2000 r·min^{-1} (the inset is the schematic of the spin coating process as 2000 r·min^{-1}), (C) AFM image of thin films prepared at 600 r·min^{-1} (the inset is the schematic of the spin coating process as 600 r·min^{-1}).

(B, C) are reprinted with permission from Ref.92, Copyright 2008 American Institute of Physics.

(RHE), representing a strong dependence and influence on the spin speed.

3.2 CVD graphene transferred or grown on target substrates

Until now, metal-catalyzed CVD method has been widely employed for the scalable production of high-quality graphene, which makes use of the pyrolysis of hydrocarbon compounds on the surface of a metal catalyst (e.g., Ni[94] and Cu[95]) at high temperatures[86]. However, the as-prepared graphene growing on the metals should be transferred onto target substrates to constitute desirable electrodes for electrochemical or photoelectrochemical applications. The common used method for transferring CVD graphene is to etch away the metal substrate using a suitable etchant. For instance, Qiu *et al.*[96] have removed CVD graphene from Cu foil with $FeCl_3$ as an etching agent, obtaining the graphene film on the surface of $FeCl_3$ solution. After that, the graphene film is carefully transferred to deionized water to remove the adsorbed ions. Lastly, the graphene is transferred onto pre-cleaned FTO glass and dried at 120 °C for 3 h under vacuum. Seo *et al.*[97] have grown single-layer graphene on Cu foil by CVD and then spin-coated Poly(-methyl methacrylate) (PMMA) on to graphene. Cu foil is etched away in ammonium persulfate (APS) solution and graphene/PMMA stacks are transferred onto SiO_2/Si substrate after cleaning in deionized water. Finally, PMMA is removed by acetone. Furthermore, a novel electrochemical bubbling method for transferring single graphene grains and graphene films to arbitrary substrates has been reported by Cheng's group, as illustrated in Fig.5 [98]. The specific processes are that: (a) the graphene grown on Pt substrate is spin-coated with PMMA and cured at 180 °C for 30 min; (b) the PMMA/graphene/Pt is used as a cathode and a Pt foil is used as an anode in a 1 mol·L^{-1} NaOH aqueous solution under a constant current of 1 A; (c) the PMMA/graphene is gradually separated from the Pt substrate driven by the H_2 bubbles produced at the cathode after applying a constant current. These complicated and skilled transfer processes, either chemical etching or electrochemical bubbling, face up with some problems, e.g., high cost, residual contamination, surface wrinkles and breakage of graphene samples, greatly compromising the material performance[86,99].

Nowadays, the advanced strategies for direct CVD graphene growth on target semiconductors and dielectrics for transfer-free fabrication of electrodes are investigated and developed. Chiu *et al.*[100] have grown graphene on silicon oxides (SiO_2) by remote catalyzation using floating Cu and H atoms for the decomposition of hydrocarbons in the CVD process, rather than using Cu foils as substrates **(**Fig.6A**)**. The defect density of the resulting graphene layers can be significantly reduced by tuning growth parameters such as the gas ratios, Cu surface areas, and substrate-to-Cu distance. Wee *et al.*[101] have developed a plasma-enhanced CVD (PECVD) growth method for high-quality graphene at low temperature, in which a H_2 plasma is introduced to etch graphene from the edges and C_2H_4 or CH_4 is used as the carbon source during graphene growth (Fig.6B). As illustrated in Fig.6(C–F**)**, graphene nanoclusters are used as the growth seeds and hexagonal graphene crystals (HGCs) are produced on SiO_2/Si. Apart from growth of graphene on conventional silicon-based substrates, Zhang *et al.*[102] have realized that epitaxial growth of graphene on hexagonal boron nitride (h-BN) at a low temperature (~500 ° C) through a remote plasma-enhanced CVD (R-PECVD) process (Fig.6G). These novel methods can directly produce high-quality graphene electrodes but the condition is too strict and complicated to be generally applied upon various and normal martials as substrates, which deserves ongoing efforts for further exploration.

3.3 Electrophoretic and electrodeposition methods

The electrophoretic deposition (EPD) is a versatile processing technique applied to deposit graphene with controllable thickness and homogeneous structure on a wide range of substrates[103]. Generally, an anode and a cathode are

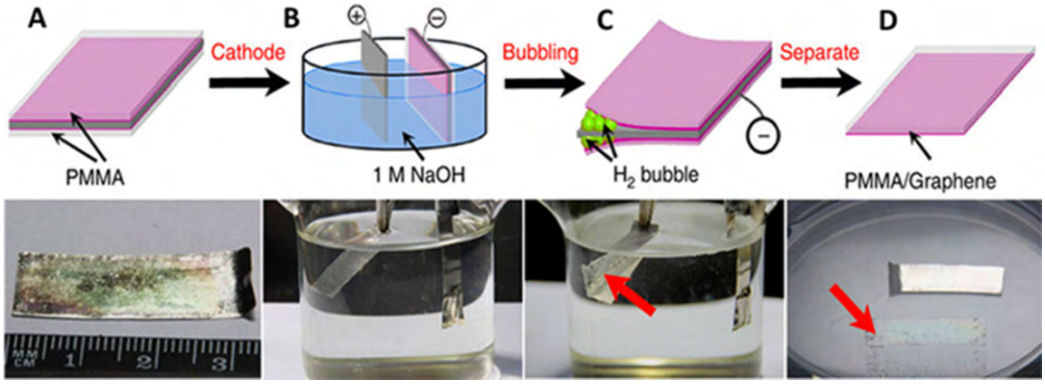

Fig.5 Schematic illustration of the graphene transfer process by electrochemical bubbling method.

(A) A Pt foil with grown graphene covered by a PMMA layer, (B) The PMMA/graphene/Pt in (A) is used as a cathode and a Pt foil is used as an anode, (C) The PMMA/graphene is gradually separated from the Pt substrate driven by the H_2 bubbles produced at the cathode after applying a constant current, (D) The completely separated PMMA/graphene layer and Pt foil after bubbling for tens of seconds. The PMMA/graphene layer is denoted by a red arrow in (C) and (B). (A–D) are reprinted with permission from Ref.98, Copyright 2012 Nature Publishing group.

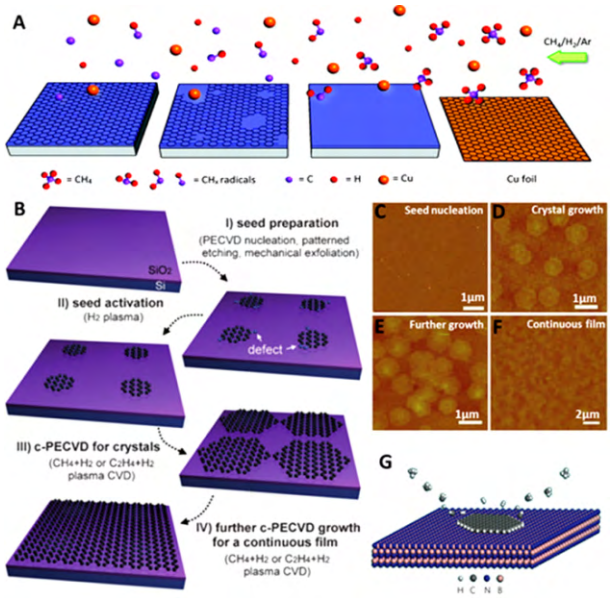

Fig.6 (A) Schematic illustration of graphene growth mechanism involving decomposition of CH_4 by floating Cu and H, sublimation of Cu particles from the Cu foil at 1000 °C, and growth of graphene on SiO_2 substrates after obtaining a certain distance from the Cu foil, (B) Schematic illustration of the PECVD procedure, (C) AFM image of the graphitic clusters after nucleation at 650 °C. AFM images of the HGCs on SiO_2 /Si after PECVD (CH_4 + H_2) growth at 600 °C for (D) 90 min and (E) for 120 min, (F) AFM image of a graphene membrane on SiO_2/Si, (G) Schematic illustration of the growth mechanism on h-BN.

(A) is reprinted with permission from Ref.100, Copyright 2012 American Chemical Society. (B–F) are reprinted with permission from Ref.101, Copyright 2013 John Wiley & Sons, Inc. (G) is reprinted with permission from Ref.102, Copyright 2013 Nature Publishing group.

vertically oriented in the stable and uniform suspension containing the charged particles or precursors for synthesis of intended electrodes. Upon applying a potential or current, target materials can be driven to migrate and deposit on the substrates by an electric filed between two electrodes. As displayed in Fig.7A, Ruoff *et al.*[104] have applied a typical EPD process to anchor overlapped and stacked RGO on the mesh stainless steel and various other electrically conductive substrates. When a direct current (DC) voltage is applied, the GO platelets migrate toward the positive electrode with the oxygen functional groups significantly removed to obtain deposited RGO on the substrate. In addition to preparing the individual RGO electrodes, the EPD method can also be used to synthesize graphene-based composites on substrates. Zhao *et al.*[105] have developed a facile EPD route to obtain the Fe_3O_4/carbon nanotubes (CNTs)/RGO composite electrode, simultaneously

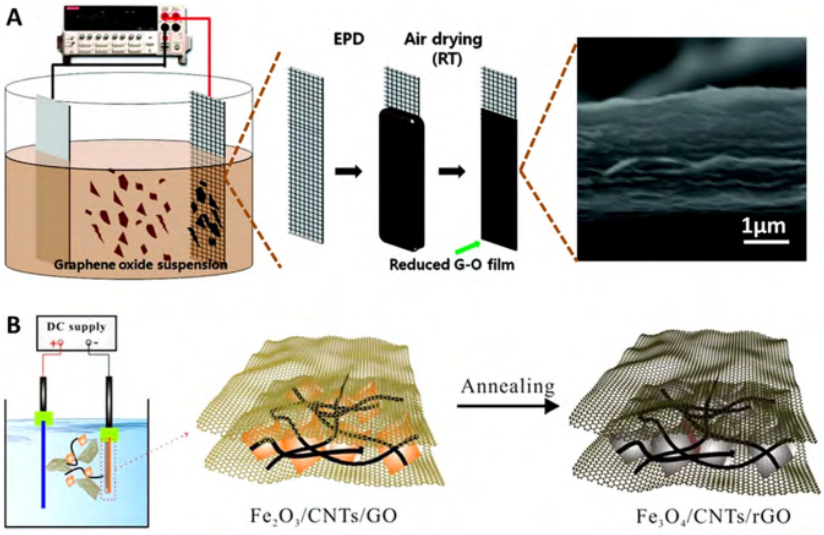

Fig.7 (A) Schematic illustration of the EPD process and cross-sectional SEM image of RGO film, (B) Schematic illustration of fabrication process for the Fe_3O_4/CNTs/RGO composite electrode.

(A) is modified with permission from Ref.104, Copyright 2010 American Chemical Society. (B) is reprinted with permission from Ref.105, Copyright 2016 American Chemical Society.

achieving material synthesis and electrode assembling (Fig.7B). In a specific experiment process, the pre-prepared GO, Fe_2O_3 nanoparticles, CNTs and I_2 are dispersed in acetone. The deposition substrate (working electrode) and the counter electrode are Cu foil and Pt plate, respectively, which are placed 1.5 cm apart. After applying a DC voltage of 100 V for 15 s, the Fe_2O_3/CNTs/GO film deposits on the Cu foil. Finally, the Fe_2O_3/CNTs/GO is transformed into final Fe_3O_4/CNTs/RGO composite electrode by heat treatment. It is noted that the success of multi-components EPD method is dependent on the same ionic charge around each component in the suspension. Herein, I_2 reacts with acetone to create protons which adsorb onto the surface of the suspended particles to make them all positively charged.

The EPD method is generally applied with high potential which in turn could influence the stability of the electrodes during processing. Applied with much lower potential than EPD method, the electrodeposition method conducts electrochemical reduction-induced formation of target materials on various substrates, in which cyclic voltammetry method is usually employed for preparation of graphene or graphene-based composite electrode[106]. Cao *et al.*[107] have performed cyclic voltammetric reduction to obtain a thin and merged graphene film on TiO_2 nanotube arrays (TNAs) (Fig.8A). Specifically, a three-electrode system is immersed into the GO dispersion. The working electrode is annealed TNAs/Ti, the counter electrode is Pt sheet, and the reference electrode is saturated calomel electrode (SCE). The scan is from –1.5 to 1 V at a rate of 50 $mV \cdot s^{-1}$ and operates with 20 cycles. The cycle numbers have a tunable effect on the surface coverage of graphene, with increased cycle numbers obtaining larger surface coverage[108]. Not only that GO in solution can be direct electrochemically reduced to yield graphene on an electrode surface by cyclic voltammetry, one-step coelectrodeposition of graphene-metal-composite films can also be obtained when both GO- and metal-reduction reactions can occur under cathodic conditions. Luo *et al.*[109] have synthesized graphene-Au composite on a glassy carbon electrode (GCE), which exhibits layered nanostructures consisting of alternating layers of Au nanoparticles (NPs) and graphene sheets, as illustrated in Fig.8B. The cyclic voltammetric reduction is performed in the deposition solutions containing 1.0 $mol \cdot L^{-1}$ GO and 100 $\mu mol \cdot L^{-1}$ tetrachloroauric acid ($HAuCl_4$) with bubbling N_2 and using a three-electrode system: a GCE as the working electrode, Pt foil as the counter electrode, and an SCE as the reference electrode. The scan is performed between −1.5 and 0.6 V at a rate of 25 $mV \cdot s^{-1}$. The metal NPs intercalation between graphene sheets not only prevents graphene agglomeration but also improves the conductivity of the graphene film.

4 Fundamental roles of graphene-based composite electrodes

4.1 Acting as dark cathodes

The graphene-metal composite is usually used as a dark cathode without demand of optical excitation while n-type semiconductor is applied as a photoanode to form a photoelectrochemical setup[19,110,111]. As a typical example, Cheng *et al.*[77,112] have conducted Pt-modified reduced graphene oxide (Pt-RGO) as cathode electrocatalyst and Pt-modified TiO_2 nanotubes (Pt-TNTs) as anode photocatalyst to establish a novel photoelectrochemical cell for converting CO_2 into C_2H_5OH, CH_3COOH, etc. (Fig.9A). The Pt-RGO composite is prepared by hydrothermal reaction with GO and $H_2PtCl_6 \cdot 6H_2O$ as precursors and then the obtained catalyst is applied onto a nickel foam. The Pt nanoparticles with a uniform size are both homogeneously dispersed on the surface of RGO and the wall of TNT, as revealed in Fig.9(B, C), respectively. In this research, the performance of photoelectrochemical reactor in the absence of CO_2 is explored and hydrogen is found to be the only product, indicating that graphene cannot produce carbonaceous products mixing with actually reduced products from CO_2. The highest carbon atom conversion rate reaches 1130 $nmol \cdot h^{-1} \cdot cm^{-2}$ with Pt-RGO catalyst, which is 6-fold and 3-fold higher than that with Pt-CNT and Pt-C catalyst, respectively (Fig.9D). A combined acid and alcohol generation

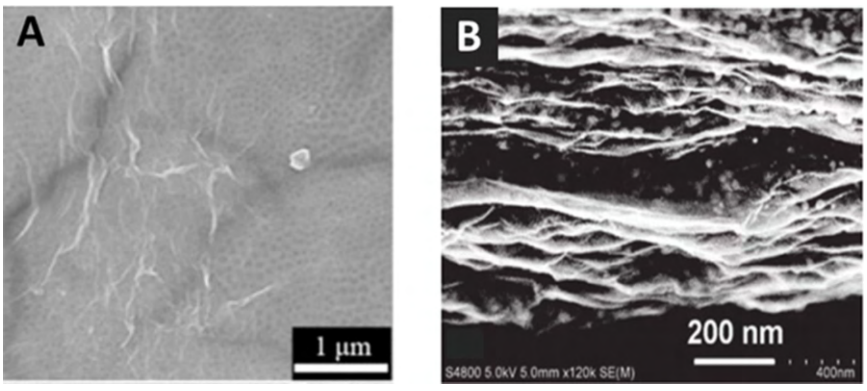

Fig.8 (A) SEM image of graphene/TNAs, (B) Cross-sectional SEM image of graphene-Au composite.

(A) is reprinted with permission from Ref.107, Copyright 2016 Elsevier. (B) is reprinted with permission from Ref.109, Copyright 2011 John Wiley & Sons, Inc.

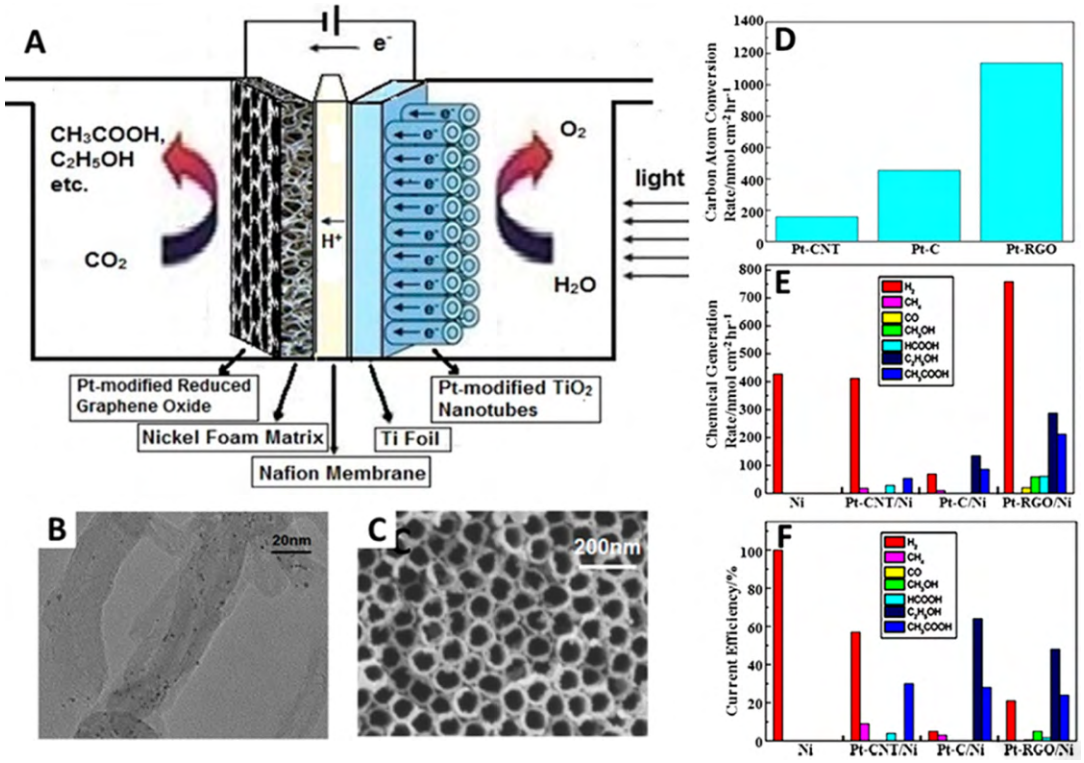

Fig.9 (A) Schematic illustration of the photoelectrochemical system, (B) TEM image of Pt-RGO, (C) SEM image of Pt-TNT, (D) Carbon atom conversion rate of CO_2 reduction under varying cathode catalysts, (E) Chemical generation rates and (F) current efficiency under varying cathodes.

(A–F) are reprinted with permission from Ref.77, Copyright 2014 American Chemical Society.

rate of 600 nmol·h^{-1}·cm^{-2} is obtained with the Pt-RGO catalyst, which is significantly higher than those with Pt-CNT [82 nmol·h^{-1}·cm^{-2}] and Pt-C [220 nmol·h^{-1}·cm^{-2}] (Fig.9E). The outstanding catalytic activity of Pt-RGO is ascribed to the fact that RGO possesses high reactant absorptivity and efficient charge transportation. On the other hand, it is noted that, as reflected in Fig.9F, the selectivity of single-carbon products (e.g., CH_3OH, HCOOH) for CO_2 reduction by Pt-RGO is still low and needs improvement in future studies.

In a subsequent work of Cheng *et al.*, they have further investigated to optimize CO_2 reduction conditions to increase carbon atom conversion, using the same Pt-RGO||Pt-TNT photoelectrochemical cell[113]. A maximum carbon atom conversion rate of 1500 nmol·h^{-1}·cm^{-2} is obtained by Pt-RGO reduction for 24 h when a 2 V voltage is applied, the catholyte pH is 8.8, and nickel foam with an average pore size of 160 μm is used as a support. Under optimum conditions, the liquid product selectivity of CO_2 reduction can reach up to 99%. And the major products of CO_2 reduction are liquid because the high specific surface area of RGO provides plenty of adsorption sites for the reactants and intermediates to favor consecutive reduction to higher-order products, such as acetic acid and ethanol. Therefore, RGO-based catalysts have potential utilization as blueprints for photoelectrochemical CO_2 reduction.

4.2 Acting as photocathode

Nanostructured hybrid assemblies that combine *p*-type inorganic semiconductors with high-conductive large surface area materials such as graphene acting as photocathode exhibit multiple favorable synergistic properties for intended applications, one of which is photoelectrochemical CO_2 reduction. Furthermore, the metal-free CO_2 reduction system is low cost, easy accessibility and environmental friendliness, compared with the systems applying rare-earth metals such as Cu, Au, Re and Rh, as well as their complexes to reduce CO_2 molecules. Nam *et al.*[78] have developed nitrogen-doped graphene quantum sheets (N-GQSs) on *p*-type silicon nanowire as heterogeneous photocathode for selective CO production in acetonitrile. The N-GQSs are synthesized by hydrothermal method and then transferred to *p*-type Si by drop casting. The current density of the N-GQSs on *p*-type Si nanowire increases gradually from the onset potential of −1.53 V *vs* Ag/Ag$^+$ and reaches 7 mA·cm^{-2} at −2.5 V *vs* Ag/Ag$^+$, which is approximately 5-fold higher than that of *p*-type Si nanowire without N-GQSs (Fig.10A). Based on the fact that approximately 75% of the electrons can be consumed for reducing CO_2 into CO on bare planar *p*-type Si electrodes, as revealed in Fig.10B, the chemical selectivity for CO is dramatically enhanced by 15% *via* decorating N-GQSs on planar *p*-type Si. And when the Si substrate is fabricated into nanowires, CO is more exclusively evolved with a selectivity of up to 95%. An isotope tracing experiment using $^{13}CO_2$ gas is

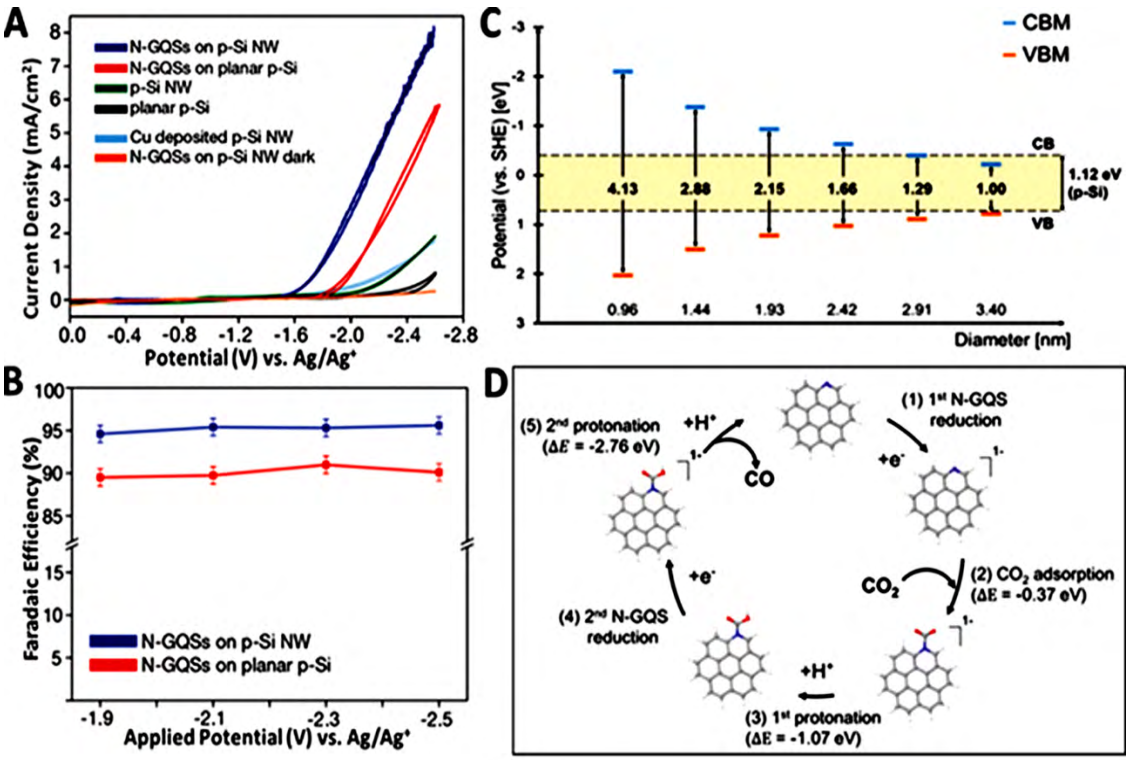

Fig.10 (A) TEM image of N-GQSs on monolayer graphene, (B) Photocurrent density-potential (J-E) curves, (C) Band alignment of *p*-type Si and calculated band edge positions of different sized GQS, (D) Proposed photoelectrocatalytic cycle of CO_2 to CO reduction on pyridinic N doped coronene ($C_{24}H_{12}$).

(A−D) are reprinted with permission from Ref.78, Copyright 2016 John Wiley & Sons, Inc.

conducted to verify the source of the evolved CO from $^{13}CO_2$ gas and not from the reduction of carbon residue or the decomposition of N-GQSs. Therefore, the N-GQSs can enhance the efficiency for reduction of CO_2 to CO, which evolves very stably on *p*-type Si nanowire with N-GQSs in wide ranges of the applied potential once the CO_2 molecule is activated.

Based on the density functional theory (DFT) calculations, the calculated band edge positions of various sizes of GQS ranging in diameter from 0.96 nm ($C_{24}H_{12}$) to 3.4 nm ($C_{294}H_{42}$) with respect to the experimental conduction band of *p*-type Si are shown in Fig.10C. The position of the conduction band minimum of GQS decreases as the diameter is increased until ~3 nm and is eventually located more negative than that of *p*-type Si when the diameter becomes larger than 3 nm. Therefore, the photoexcited electrons in *p*-type Si can be transferred to the GQS and participate in the catalytic reduction of CO_2 when the diameter is larger than 3 nm. The N dopants is also turned out to have minor effect on the band edge positions and serve as an active center for CO_2 reduction. Moreover, based on result of DFT calculations, the overall photoelectrocatalytic reduction mechanism of CO_2 to CO is summarized in Fig.10D. The specific steps are (1) the first N-GQS reduction, (2) adsorption of CO_2 to the pyridinic N site, (3) the first protonation, (4) the second N-GQS reduction, and (5) the second protonation to yield CO and H_2O.

4.3 Acting as photoanodes

Subramanian *et al.*[114] have prepared the 3D tree-like architectures as candidates of photoanodes for photoelectrochemical performance. As visually displayed in Fig.11A, a nature-inspired "tree"-like 3D hierarchical branch titania ($bTiO_2$) architecture strategically assembles reduced graphene oxide (RGO) and cadmium sulfide (CdS). An optimum loading (1 mg·mL^{-1}) of RGO boosts the photoresponse by an additional 150% compared to "CdS-only" photoanodes (Fig.11B), which is ascribed to the effective electron shuttling capability of the RGO interlayer. The on/off cycles (Fig.11C) and the *J*/*V* data (Fig.11D) synergistically manifest that the presence of RGO significantly enhances the photoelectrochemical performance of the 3D $bTiO_2$/CdS. Therefore, successful integration of RGO with other materials can facilitate more efficient charge separation leading to further increase in the photoelectrochemical performance.

Additionally, graphene can also be employed as a scaffold to create a 2D conductive support path for charge transport at the electrode surface[115]. Kamat *et al.*[116] have conducted fortification of CdSe quantum dots (QDs) with graphene oxide (GO) as photoanode in an open cell configuration, consisting of Cu_2S/RGO films as counter electrode and S^{2-}/S_n^{2-} as the redox electrolyte (Fig.12A). Submonolayer loading of CdSe QDs on typically mono- to few-layered graphene sheets is shown in Fig.12C. Both RGO and GO serve as effective quenchers of

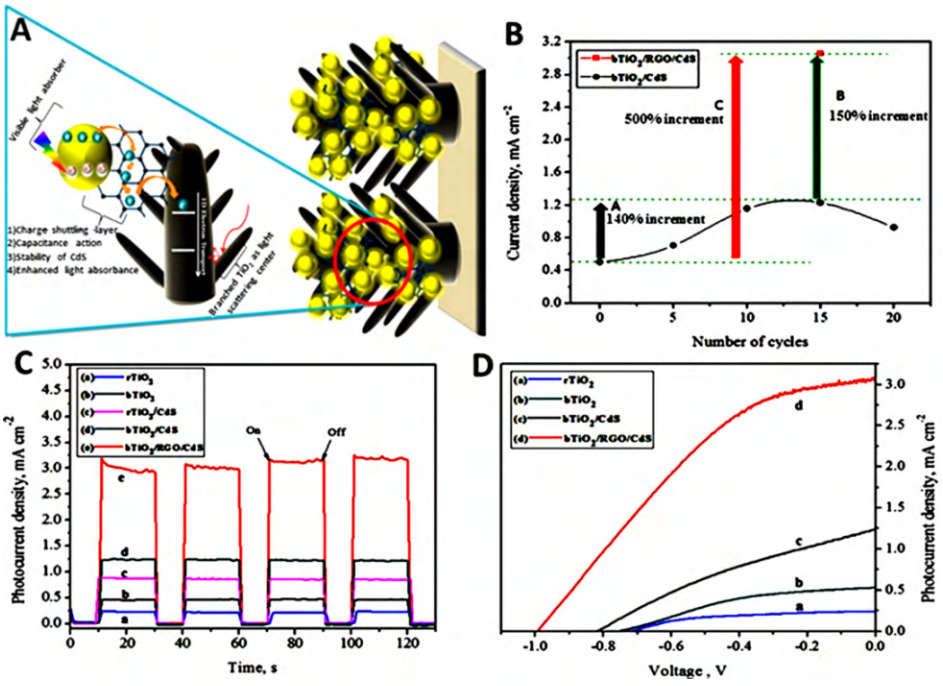

Fig.11 (A) Schematic illustration of strategic integration of the RGO with CdS over 3D TiO_2 architectures, (B) Comparative values of the stabilized peak current obtained in the photoelectrochemical measurements of panel with CdS (140% increment), RGO/CdS (150% increment) and combined effect of RGO and CdS (500% increment), Photoelectrochemical responses showing (C) the multiple "On-Off" cycles and (D) J-V characteristics ($rTiO_2$ represents TiO_2 nanorod).

(A−D) are reprinted with permission from Ref.114, Copyright 2015 American Chemical Society.

excited CdSe (Fig.12D). And GO has greater electron-accepting capacity because GO quenches more efficiently than RGO at all concentrations (inset, Fig.12D). The significant enhancement of CdSe-(R)GO photoanodes over CdSe-only film for the incident photon to current efficiencies (IPCE) is attributed to the indirect participation of (R)GO in accepting

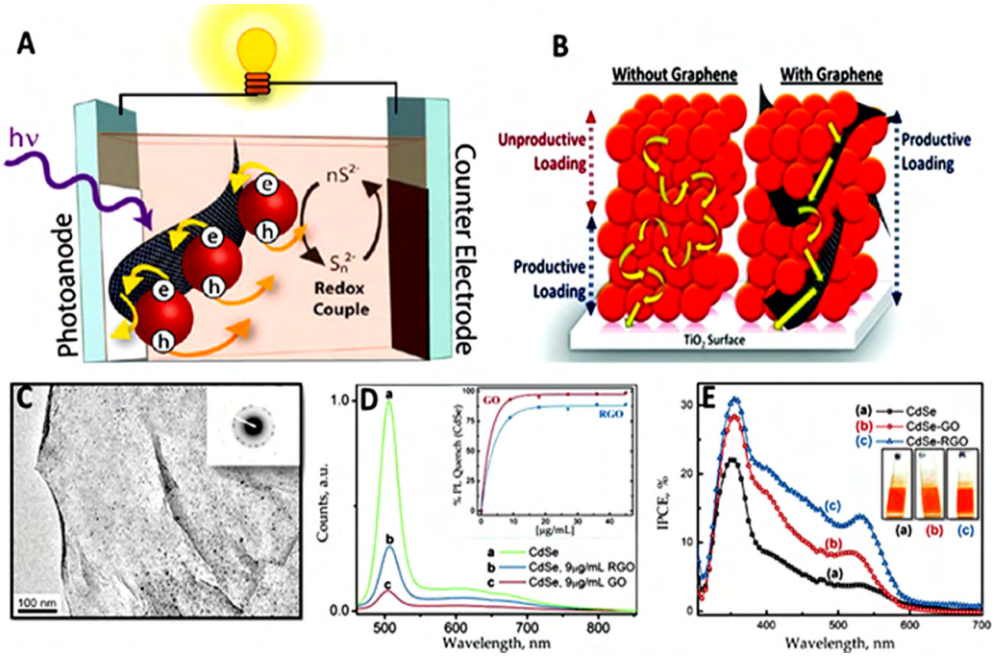

Fig.12 Schematic illustrations of (A) an open cell configuration in which CdSe QDs with graphene oxide as photoanode and (B) electron transfer pathways, (C) TEM micrograph of GO after illumination (> 420 nm) of CdSe-GO dispersion, (D) Quenching of CdSe QDs photoluminescence by GO and RGO (the inset is effective quenching even at low graphene concentration), (E) Incident photon to current efficiency (IPCE) of CdSe and CdSe-(R)GO film.

(A−E) are reprinted with permission from Ref.116, Copyright 2012 American Chemical Society.

and shuttling electrons to the electrode surface (Fig.12E). Therefore, it is schematically illustrated in Fig.12B that the random walks of electrons in CdSe QDs become sequential flow along graphene after incorporation of graphene in CdSe QDs loading. There is a new avenue opened toward the application of graphene as a scaffold to improve the charge transfer.

Inspired by aforementioned research, these superiorities of graphene can be utilized to advance photoanodes for photoelectrochemical CO_2 reduction. The graphene on anodic electrode directly influences the efficiency of water decomposition provided protons and electrons for cathode CO_2 reduction, which, in turn, affects the catalytic efficiency of anodization procedure. Therefore, although the reduction of CO_2 takes place in cathodic chamber, its efficiency is still indirectly affected by the cathodic reaction. Mat *et al*.[117] have constructed copper-doped, titanium dioxide-reduced graphene oxide (Cu-RGO-TiO_2) nanocomposite photoanode for photoelectrocatalytic reduction of CO_2 to methanol and formic acid, with a platinum (Pt) wire and a saturated calomel electrode (SCE) as the counter and reference electrode, respectively (Fig.13A). The advantages of graphene for facilitating electrons transfer and electron-hole pairs separation are indicated by the lowest emission intensity of the Cu-RGO-TiO_2 in the photoluminescence spectrum (Fig.13B) and lowest resistance of the Cu-RGO-TiO_2 in the Nyquist plots (Fig.13C) than these of RGO-TiO_2 and TiO_2.

The above works have proven the distinct superiorities and great potential of graphene applied in photoelectrochemical CO_2 reduction. When graphene-based composites act as cathode, the 2D π-conjugated structure and large surface area of graphene mainly provide more basic sites and thus facilitate CO_2 adsorption. Furthermore, the graphene mainly plays the role of electron acceptor and transporter when graphene-based composite is adopted as anode to indirectly improve the efficiency of photoelectrochemical CO_2 reduction. So far, there are no researches on the graphene-based composites as dark anodes combining with *p*-type semiconductor as photocathodes. However, many researches on the graphene-based electrodes (e.g., Co_3O_4-graphene[118], Fe_3O_4-graphene[119]) for electrochemical oxygen evolution reaction (OER) of water have been reported, indicating that graphene-based composites have promising potential of acting as dark anodes with proper photocathodes in photoelectrochemical system.

5 Potential research categories for photoelectrochemical applications

Photoelectrochemical catalysis, synergistically integrated electrochemical and photocatalytic methods, possesses two advantages:[120] (i) the application of certain electrode potential not only drives specific electrode reaction but also facilitates the separation of photoinduced carriers, enhancing photocatalytic process; (ii) the assistance of light irradiation lowers the electrochemical barrier and promotes the electrode kinetics for a specific reaction, favoring the electrochemical process. Therefore, with regard to the superiorities of photoelectrochemical system, we discuss the strategies about evolution of potential photocatalytic and electrocatalytic system into photoelectrochemical applications for CO_2 reduction on the basis of their common characteristics, which are not limited to only graphene-based composite electrode and able to extend researches on photoelectrochemical CO_2

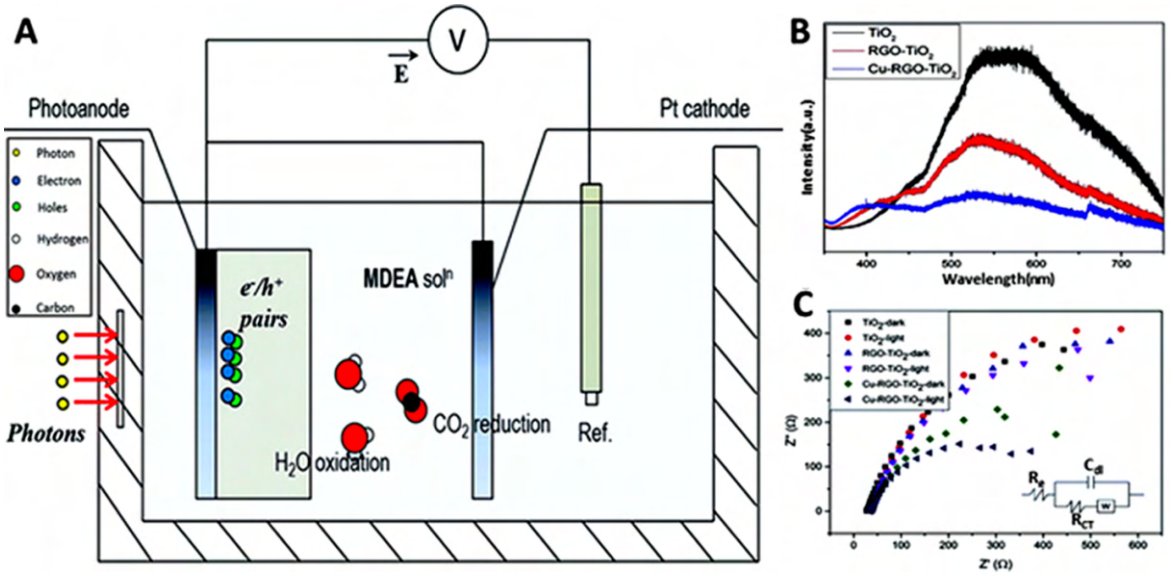

Fig.13 (A) Schematic illustration of photoelectrochemical reactor, (B) Photoluminescence spectrum of TiO_2, RGO-TiO_2 and Cu-RGO-TiO_2, (C) Nyquist plots of the TiO_2, RGO-TiO_2 and Cu-RGO-TiO_2 film electrodes at open circuit potentials both in the dark and under visible irradiation (the inset is the equivalent circuit).

(A−C) are reprinted with permission from Ref.117, Copyright 2015 Royal Society of Chemistry.

reduction system.

5.1 Potential *Z*-scheme photocatalytic systems

Z-scheme photocatalysis system mimicking plant photosynthesis has become a novel artificial two-step photosynthetic system, whose processes occur simultaneously in time but separately in space[121,122]. The *Z*-scheme system containing *p*-type and *n*-type semiconductors is an indispensable factor for evolution of photoelectrochemical system, possessing a similar electron flow. Specifically, after both semiconductors are stimulated by light, the photogenerated electrons in an O_2-evolving side are migrated to combine with the holes in a CO_2-reducting side, remaining the holes in the O_2-evolving side and electrons in the CO_2-reducting side to participate in following reaction[123]. The distinction between the two systems is the way of electrons migration. In a *Z*-scheme system, it can happen at contact interface of the two semiconductors or electron mediators (e.g., graphene[124,125]) between the two semiconductors while in a photoelectrochemical system, the electrons are commonly migrated through external wire connecting the two semiconductors[126,127]. Therefore, properly changing the way of electrons migration is feasible for the *Z*-scheme photocatalysis system to be evolved as a newly designed photoelectrochemical setup, which can be categorized as type III discussed in Section 2.2.

Arai *et al.* have investigated the *Z*-scheme system to be tuned as photoelectrochemical system[128]. The total reaction mechanism of the *Z*-scheme system is shown in Fig.14A, including the SC_{RED}/[MCP] (Metal Complex Polymer) photocatalyst for CO_2 reduction and the SC_{OX} photocatalyst for H_2O oxidation (SC_{RED} and SC_{OX} denote semiconductors at the sites of the reduction and oxidation, respectively)[129]. Based on the *Z*-scheme photocatalysis system, herein, a wired two-compartment quartz cell is conducted for photoelectrochemical reduction of CO_2 into formate, combining the reduced $SrTiO_3$ (r-STO) photoanode with the InP/[RuCP] (Ruthenium Complex Polymer) photocathode (Fig.14B)[78]. After 3-hour irradiation of simulated solar lights, the obtained conversion efficiency from solar energy to formate is ca. 0.14%, indicating the photoelectrochemical system transferred from Z-scheme system can well work and realize the reduction of CO_2. Kudo *et al.*[130] have fabricated a *Z*-scheme system in which a visible-light-driven CoO_x-loaded $BiVO_4$ as an O_2-evolving photocatalyst, metal sulfide as a H_2-evolving and CO_2-reducing photocatalyst, and RGO as an efficient electron mediator (Fig.15A). On the basis of this *Z*-scheme system and $Pt/CuGaS_2$ and $CoO_x/BiVO_4$ as *p*-type and *n*-type semiconductors, $Pt/CuGaS_2$ and $CoO_x/BiVO_4$ are respectively applied as cathodic and anodic photoelectrodes to form a photoelectrochemical system. The photogenerated electrons flow from the conduction band of $BiVO_4$ to external wire and finally to the valence band of $CuGaS_2$ after light irradiation. Then, the flowing electrons are combined with the holes generated form $CuGaS_2$ and the paired electrons are motivated to the conduction band of $CuGaS_2$ to participate in following reaction (Fig.15B). Because Pt-cocatalyst works as active sites for photocatalytic H_2 generation, the photoelectrochemical system primarily works for H_2 evolution without an external bias.

These results have indicated that the *Z*-scheme system containing *p*-type and *n*-type semiconductors is feasible and potential to be conducted as a newly-designed photoelectrochemical system. The photocatalytic system commonly utilizes a suspension of photocatalyst particles in a solvent for the reduction of dissolved CO_2 [49]. In this regard, the technological barrier for this kind of transformation is to make the dispersed particle anchor on conducted electrode. The physical coating methods (i.e., dip-coating, drop-casting and spin-coating) discussed in Section 3.1 may be the most convenient and efficient approaches and still deserve further exploration.

5.2 Potential electrocatalytic systems

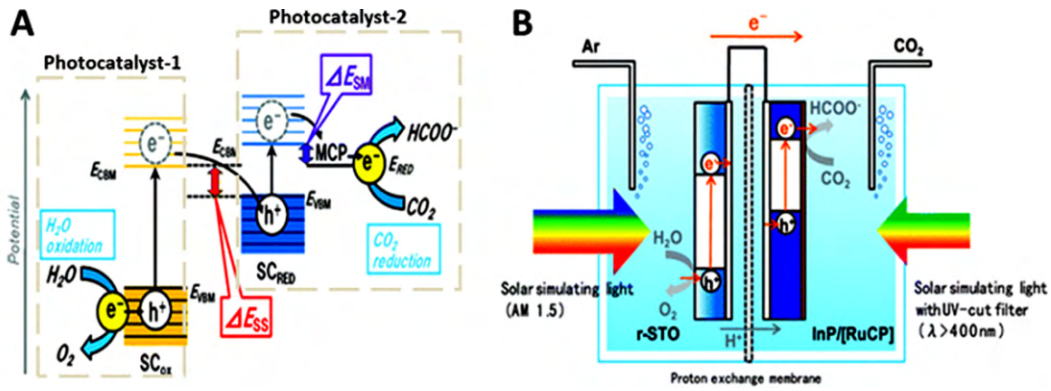

Fig.14 Schematic illustrations of (A) *Z*-scheme system for CO_2 reduction and H_2O oxidation, and (B) the photoelectrochemical reduction of CO_2 with a two-electrode configuration and no electrical bias.

(A, B) are reprinted with permission from Ref.128, Copyright 2013 Royal Society of Chemistry.

The electrochemical CO_2 reduction has triggered a large number of researches for three decades. There are three typical cells used for electrochemical CO_2 conversions in laboratory, which are schematically summarized in Fig.16 [131]. Particularly, the setup in Fig.16B is similar to the configuration of photoelectrochemical CO_2 reduction, with anodic and cathodic chambers separated by an H^+-conducting membrane. Besides, for photoelectrocatalytic applications, an artificial lamp source or a solar simulator[111] is installed outside of the reactor and the light passes through the quartz window embedded in the wall. There is an exception that a UV lamp can be located in internal configuration[132].

It is typical for both electrochemical and photoelectrochemical reactors that the separated non-direct reactions in two compartments permit researchers to tailor the properties needed for each redox process independently. Furthermore, considering the similarity of their setups, electrocatalytic reactor is able to be combined with half-cell photoelectrochemical reactor in separated compartments. Centi *et al.*[52] have successfully conducted a continuous flow electrocatalytic reactor simulating the anode part of the photoelectrochemical reactor. The Pt nanoparticles on carbon-based electrodes are used to electrochemical reduction integrating TiO_2 photoanode to ultimately use solar energy and water to convert CO_2 to long carbon-chain hydrocarbons at room temperature and atmospheric pressure.

Using the conventional liquid phase electrochemical approach, many problems exist including the solubility of CO_2, the formation of products type, etc.[19]. To overcome these problems, gas phase electrocatalytic reduction of CO_2 is applied with a gas diffusion electrode (GDE), as displayed in Fig.16C**.** Interestingly, the anodic chamber filled with electrolyte is able to simulate the half-cell of the photoelectrochemical device. Perathoner *et al.*[133] have proposed a novel concept based on a gas-phase photoelectrochemical device. The electrocatalyst is the Pt supported on carbon nanotubes, which is then deposited on a conductive carbon cloth to allow the electrical contact and the diffusion of gaseous CO_2. Photocatalytic anode is composed of a nanostructured TiO_2-based thin film, where H_2O is splitted to produce O_2 and protons. The CO_2 in gas phase is reduced by protons passing through a Nafion membrane from the photocatalytic side and electrons from the wire. This device, which is different from the conventional liquid phase electrochemical and photoelectrochemical approach, is able to form long-chain hydrocarbons at room temperature. Therefore, depending on their distinguishing features for dual-chamber, it is feasible to take advantage of half-cell photoelectrochemical application combined with electrochemical setup to obtain a desirable and further tunable performance for photoelectrochemical CO_2

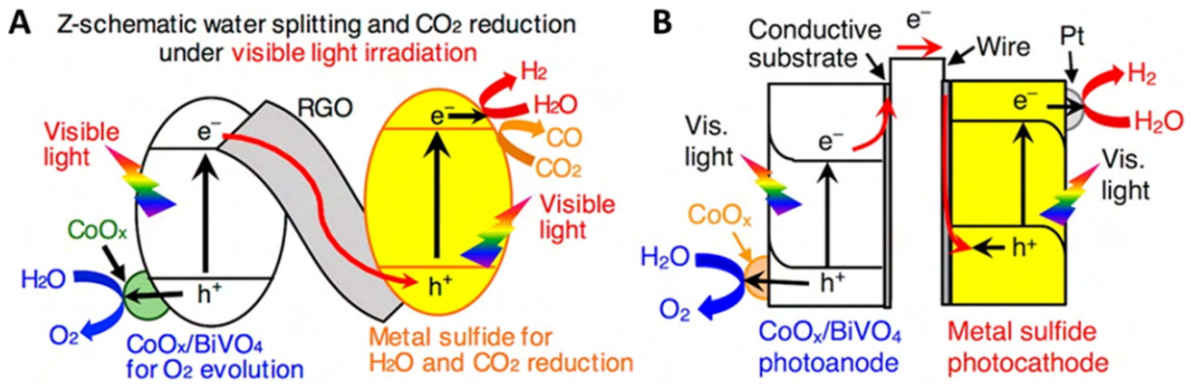

Fig.15 Schematic illustrations of (A) *Z*-scheme system for water splitting and CO_2 reduction and (B) photoelectrochemical system consisting of a metal sulfide photocatalyst electrode with a p-type semiconductor character and a $CoO_x/BiVO_4$ photoelectrode.

(A, B) are reprinted with permission from Ref.130, Copyright 2016 American Chemical Society.

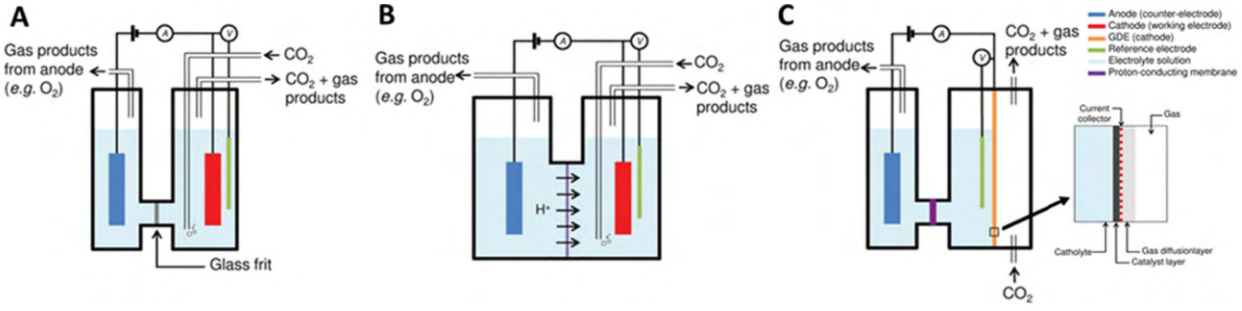

Fig.16 Laboratory cells used for electrochemical CO_2 conversion: (A) two-compartment cell, (B) cell with electrodes separated by an H^+-conducting membrane, and (C) cell with a gas diffusion electrode.

(A−C) are reprinted with permission from Ref.131, Copyright 2013 Royal Society of Chemistry.

reduction, which is not limited to only graphene-based composite materials.

6 Conclusions and perspectives

In this review, we elaborate the basic principle and highlight the recent progress in developing efficient graphene-based composites for photoelectrochemical CO_2 reduction. The basic preparation methods for graphene or graphene-based composite (photo)electrodes are summarized. The role of graphene can be excellent CO_2 absorber and electrons transfer media, which could significantly improve efficiency of the relevant (photo)anode or (photo)cathode. We have also demonstrated the potential photocatalytic and electrochemical systems that could be evolved to photoelectrochemical application for CO_2 reduction, which will further advance our graphene-based composite systems toward improving the efficiency of photoelectrochemical reduction of CO_2. After all the researches in this field are at an early stage, there exist a number of challenges in the exploitation of highly activity graphene-based composites for photoelectrochemical CO_2 reduction.

To further develop the application of graphene-based composite electrodes in photoelectrochemical reduction of CO_2, ongoing efforts could be devoted to the following aspects. (i) More explorations are needed to achieve more comprehensive understanding of the rationales of photoelectrochemical CO_2 reduction over graphene and thus to better control the pathways of CO_2 reduction and utilize the traits of graphene more felicitously. (ii) Besides performing as CO_2 absorber and conductive media, graphene possesses other excellent properties widely acknowledged in photocatalytic filed, such as band gap tuning and the macromolecular photosensitizer role. To make full use of its advantages to tune photoelectrochemical CO_2 reduction, further investigations are imperative on the basis of achievements about fundamental roles of graphene in the graphene-based composite photocatalysts. (iii) To fabricate higher-performance graphene-based composite electrodes, a system-level engineering needs to be optimized, including controlling morphologies and structures at the nanoscale, tailoring the interface and interactions among graphene and targeted materials. Regarding the overall photoelectrochemical performance, it is essential to achieve the harmonious combination of each component to maximally optimize the functional electrodes. (iv) The existing preparation methods of graphene-based composite electrodes deserve improvement to optimize the thickness, homogeneity and stability of the materials and thus to tune the performance of photoelectrochemical CO_2 reduction. (v) The tailored graphene materials, such as zero-dimensional graphene quantum dots, one-dimensional graphene nanoribbons and three-dimensional graphene frameworks show a variety of fascinating features, thereby offering a fertile and flexible ground for the further development of graphene-based photoelectrochemical catalysis for CO_2 reduction.

With regard to the implementation of potential photocatalysts and electrocatalysts into newly-designed photoelectrochemical applications, the equilibrium between enhanced efficiency and the cost is ought to be concerned because the complicacy and costing of photoelectrochemical applications are higher than those of sole photocatalytic and electrocatalytic ones. Being cost-effective is a current key issue to further optimize the stable, efficient, safe photoelectrochemical system. Taking advantage of the nature solar light instead of artificial lamp sources enables the energy saving, cost reduction and environmentally friendly. Therefore, a solar-driven photoelectrochemical-based CO_2 reduction device is a promising development trend toward a sustainable system in the future.

References

(1) Luthi, D.; Le Floch, M.; Bereiter, B.; Blunier, T.; Barnola, J. M.; Siegenthaler, U.; Raynaud, D.; Jouzel, J.; Fischer, H.; Kawamura, K.; Stocker, T. F. *Nature* **2008,** *453*, 379. doi: 10.1038/nature06949

(2) Canadell, J. G.; Le Quere, C.; Raupach, M. R.; Field, C. B.; Buitenhuis, E. T.; Ciais, P.; Conway, T. J.; Gillett, N. P.; Houghton, R. A.; Marland, G. *Proc. Natl. Acad. Sci. U. S. A.* **2007,** *104*, 18866. doi: 10.1073/pnas.0702737104

(3) Somorjai, G. A.; Frei, H.; Park, J. Y. *J. Am. Chem. Soc.* **2009,** *131*, 16589. doi: 10.1021/ja9061954

(4) Aresta, M.; Dibenedetto, A. *Dalton Trans.* **2007,** 2975. doi: 10.1039/B700658F

(5) Centi, G.; Perathoner, S. *Catal. Today* **2009,** *148*, 191. doi: 10.1016/j.cattod.2009.07.075

(6) Jiang, Z.; Xiao, T.; Kuznetsov, V. L.; Edwards, P. P. *Philos. Trans. R. Soc. A* **2010,** *368*, 3343. doi: 10.1098/rsta.2010.0119

(7) Grills, D. C.; Fujita, E. *J. Phys. Chem. Lett.* **2010,** *1*, 2709. doi: 10.1021/jz1010237

(8) Bolton, J. R. *Science* **1978,** *202*, 705. doi: 10.1126/science.202.4369.705

(9) Ikeue, K.; Yamashita, H.; Anpo, M.; Takewaki, T. *J. Phys. Chem. B* **2001,** *105*, 8350. doi: 10.1021/jp010885g

(10) Varghese, O. K.; Paulose, M.; LaTempa, T. J.; Grimes, C. A. *Nano Lett.* **2009,** *9*, 731. doi: 10.1021/nl803258p

(11) Dimitrijevic, N. M.; Vijayan, B. K.; Poluektov, O. G.; Rajh, T.; Gray, K. A.; He, H.; Zapol, P. *J. Am. Chem. Soc.* **2011,** *133*, 3964. doi: 10.1021/ja108791u

(12) Liu, Q.; Zhou, Y.; Kou, J.; Chen, X.; Tian, Z.; Gao, J.; Yan, S.; Zou, Z. *J. Am. Chem. Soc.* **2010,** *132*, 14385. doi: 10.1021/ja1068596

(13) Izumi, Y. *Coord. Chem. Rev.* **2013,** *257*, 171. doi: 10.1016/j.ccr.2012.04.018

(14) Fu, Y.; Sun, D.; Chen, Y.; Huang, R.; Ding, Z.; Fu, X.; Li, Z. *Angew. Chem.* **2012,** *51*, 3420. doi: 10.1002/anie.201108357

(15) Roy, S. C.; Varghese, O. K.; Paulose, M.; Grimes, C. A. *ACS Nano* **2010,** *4*, 1259. doi: 10.1021/nn9015423

(16) Benson, E. E.; Kubiak, C. P.; Sathrum, A. J.; Smieja, J. M. *Chem. Soc. Rev.* **2009,** *38*, 89. doi: 10.1039/B804323J

(17) Spinner, N. S.; Vega, J. A.; Mustain, W. E. *Catal. Sci. Technol.* **2012,** *2*, 19. doi: 10.1039/C1CY00314C

(18) Li, C. W.; Kanan, M. W. *J. Am. Chem. Soc.* **2012,** *134*, 7231. doi: 10.1021/ja3010978

(19) Ampelli, C.; Centi, G.; Passalacqua, R.; Perathoner, S. *Energy Environ. Sci.* **2010,** *3*, 292. doi: 10.1039/B925470F

(20) Bard, A. J. *Science* **1980,** *207*, 139. doi: 10.1126/science.207.4427.139

(21) Sato, S.; Arai, T.; Morikawa, T. *Inorg. Chem.* **2015,** *54*, 5105. doi: 10.1021/ic502766g

(22) Halmann, M. *Nature* **1978,** *275*, 115. doi: 10.1038/275115a0

(23) Sato, S. Photoelectrochemical CO_2 Reduction. In *Encyclopedia of Applied Electrochemistry*; Springer New York: 2014; pp 1535.

(24) Li, D.; Kaner, R. B. *Science* **2008,** *320*, 1170. doi: 10.1126/science.1158180

(25) Li, Y.; Su, H.; Chan, S. H.; Sun, Q. *ACS Catal.* **2015,** *5*, 6658. doi: 10.1021/acscatal.5b01165

(26) Yang, M. Q.; Xu, Y. J. *Nanoscale Horiz.* **2016,** *1*, 185. doi: 10.1039/C5NH00113G

(27) Zhu, D. D.; Liu, J. L.; Qiao, S. Z. *Adv. Mater.* **2016,** *28*, 3423. doi: 10.1002/adma.201504766

(28) Xiao, F. X.; Miao, J.; Liu, B. *J. Am. Chem. Soc.* **2014,** *136*, 1559. doi: 10.1021/ja411651e

(29) Liu, Q.; Liu, Z.; Zhang, X.; Yang, L.; Zhang, N.; Pan, G.; Yin, S.; Chen, Y.; Wei, J. *Adv. Funct. Mater.* **2009,** *19*, 894. doi: 10.1002/adfm.200800954

(30) Zhai, C.; Zhu, M.; Lu, Y.; Ren, F.; Wang, C.; Du, Y.; Yang, P. *Phys. Chem. Chem. Phys.* **2014,** *16*, 14800. doi: 10.1039/C4CP01401D

(31) Chang, H.; Lv, X.; Zhang, H.; Li, J. *Electrochem. Commun.* **2010,** *12*, 483. doi: 10.1016/j.elecom.2010.01.025

(32) Xiang, Q.; Cheng, B.; Yu, J. *Angew. Chem. Int. Ed.* **2015,** *54*, 11350. doi: 10.1002/anie.201411096

(33) Tran, P. D.; Wong, L. H.; Barber, J.; Loo, J. S. C. *Energy Environ. Sci.* **2012,** *5*, 5902. doi: 10.1039/C2EE02849B

(34) Habisreutinger, S. N.; Schmidt-Mende, L.; Stolarczyk, J. K. *Angew. Chem. Int. Ed.* **2013,** *52*, 7372. doi: 10.1002/anie.201207199

(35) Li, H.; Gan, S.; Wang, H.; Han, D.; Niu, L. *Adv. Mater.* **2015,** *27*, 6906. doi: 10.1002/adma.201502755

(36) Sato, S.; Arai, T.; Morikawa, T.; Uemura, K.; Suzuki, T. M.; Tanaka, H.; Kajino, T. *J. Am. Chem. Soc.* **2011,** *133*, 15240. doi: 10.1021/ja204881d

(37) Magesh, G.; Kim, E. S.; Kang, H. J.; Banu, M.; Kim, J. Y.; Kim, J. H.; Lee, J. S. *J. Mater. Chem. A* **2014,** *2*, 2044. doi: 10.1039/C3TA14408A

(38) Chen, W. Y.; Mattern, D. L.; Okinedo, E.; Senter, J. C.; Mattei, A. A.; Redwine, C. W. *AIChE J.* **2014,** *60*, 1054. doi: 10.1002/aic.14347

(39) Xie, S.; Zhang, Q.; Liu, G.; Wang, Y. *Chem. Commun.* **2016,** *52*, 35. doi: 10.1039/C5CC07613G

(40) Tinnemans, A.; Koster, T.; Thewissen, D.; Mackor, A. *Recl. Trav. Chim. Pays-Bas* **1984,** *103*, 288. doi: 10.1002/recl.19841031004

(41) Zhao, W. W.; Xiong, M.; Li, X. R.; Xu, J. J.; Chen, H. Y. *Electrochem. Commun.* **2014,** *38*, 40. doi: 10.1016/j.elecom.2013.10.035

(42) Li, X.; Wen, J.; Low, J.; Fang, Y.; Yu, J. *Sci. China Mater.* **2014,** *57*, 70. doi: 10.1007/s40843-014-0003-1

(43) Schouten, K. J. P.; Kwon, Y.; van der Ham, C. J. M.; Qin, Z.; Koper, M. T. M. *Chem. Sci.* **2011,** *2*, 1902. doi: 10.1039/C1SC00277E

(44) Inoue, T.; Fujishima, A.; Konishi, S.; Honda, K. *Nature* **1979,** *277*, 637. doi: 10.1038/277637a0

(45) Anpo, M.; Yamashita, H.; Ichihashi, Y.; Ehara, S. *J. Electroanal. Chem.* **1995,** *396*, 21. doi: 10.1016/0022-0728(95)04141-A

(46) Yang, C. C.; Vernimmen, J.; Meynen, V.; Cool, P.; Mul, G. *J. Catal.* **2011,** *284*, 1. doi: 10.1016/j.jcat.2011.08.005

(47) Ulagappan, N.; Frei, H. *J. Phys. Chem. A* **2000,** *104*, 7834. doi: 10.1021/jp001470i

(48) Amatore, C.; Saveant, J. M. *J. Am. Chem. Soc.* **1981,** *103*, 5021. doi: 10.1021/ja00407a008

(49) Chang, X.; Wang, T.; Gong, J. *Energy Environ. Sci.* **2016,** *9*, 2177. doi: 10.1039/C6EE00383D

(50) Hori, Y.; Wakebe, H.; Tsukamoto, T.; Koga, O. *Electrochim. Acta* **1994,** *39*, 1833. doi: 10.1016/0013-4686(94)85172-7

(51) Koppenol, W. H.; Rush, J. D. *J. Phys. Chem.* **1987,** *91*, 4429. doi: 10.1021/j100300a045

(52) Centi, G.; Perathoner, S.; Wine, G.; Gangeri, M. *Green Chem.* **2007,** *9*, 671. doi: 10.1039/B615275A

(53) Wu, T.; Zou, L.; Han, D.; Li, F.; Zhang, Q.; Niu, L. *Green Chem.* **2014,** *16*, 2142. doi: 10.1039/C3GC42454E

(54) Ong, W. J.; Tan, L. L.; Chai, S. P.; Yong, S. T. *Chem. Commun.* **2015,** *51*, 858. doi: 10.1039/C4CC08996K

(55) Yu, J.; Jin, J.; Cheng, B.; Jaroniec, M. *J. Mater. Chem. A* **2014,** *2*, 3407. doi: 10.1039/C3TA14493C

(56) Stoller, M. D.; Park, S.; Zhu, Y.; An, J.; Ruoff, R. S. *Nano Lett.* **2008,** *8*, 3498. doi: 10.1021/nl802558y

(57) Gattrell, M.; Gupta, N.; Co, A. *J. Electroanal. Chem.* **2006,** *594*, 1. doi: 10.1016/j.jelechem.2006.05.013

(58) Yoneyama, H.; Sugimura, K.; Kuwabata, S. *J. Electroanal. Chem.* **1988,** *249*, 143. doi: 10.1016/0022-0728(88)80355-3

(59) Chang, X.; Wang, T.; Zhang, P.; Wei, Y.; Zhao, J.; Gong, J. *Angew. Chem. Int. Ed.* **2016,** *128*, 8986. doi: 10.1002/anie.201602973

(60) Allam, N. K.; Shankar, K.; Grimes, C. A. *J. Mater. Chem.* **2008,** *18*, 2341. doi: 10.1039/B718580D

(61) Luo, J.; Im, J. H.; Mayer, M. T.; Schreier, M.; Nazeeruddin, M. K.; Park, N. G.; Tilley, S. D.; Fan, H. J.; Grätzel, M. *Science* **2014,** *345*, 1593. doi: 10.1126/science.1258307

(62) Minguez-Bacho, I.; Courte, M.; Fan, H. J.; Fichou, D. *Nanotechnology* **2015,** *26*, 185401. doi: 10.1088/0957-4484/26/18/185401

(63) Chua, L. L.; Zaumseil, J.; Chang, J. F.; Ou, E. C. W.; Ho, P. K. H.; Sirringhaus, H.; Friend, R. H. *Nature* **2005,** *434*, 194. doi: 10.1038/nature03376

(64) Koval, C. A.; Howard, J. N. *Chem. Rev.* **1992,** *92*, 411. doi: 10.1021/cr00011a004

(65) Gao, Y. Q.; Georgievskii, Y.; Marcus, R. A. *J. Chem. Phys.* **2000,** *112*, 3358. doi: 10.1063/1.480918

(66) White, J. L.; Baruch, M. F.; Pander Iii, J. E.; Hu, Y.; Fortmeyer, I. C.; Park, J. E.; Zhang, T.; Liao, K.; Gu, J.; Yan, Y.; Shaw, T. W.; Abelev, E.; Bocarsly, A. B. *Chem. Rev.* **2015,** *115*, 12888. doi: 10.1021/acs.chemrev.5b00370

(67) Peng, Y. P.; Yeh, Y. T.; Shah, S. I.; Huang, C. P. *Appl. Catal., B* **2012,** *123–124*, 414. doi: 10.1016/j.apcatb.2012.04.037

(68) Chen, D.; Zhang, H.; Liu, Y.; Li, J. *Energy Environ. Sci.* **2013,** *6*, 1362. doi: 10.1039/c3ee23586f

(69) Lightcap, I. V.; Kamat, P. V. *Acc. Chem. Res.* **2013,** *46*, 2235. doi: 10.1021/ar300248f

(70) Low, J.; Yu, J.; Ho, W. *J. Phys. Chem. Lett.* **2015,** *6*, 4244. doi: 10.1021/acs.jpclett.5b01610

(71) Lightcap, I. V.; Murphy, S.; Schumer, T.; Kamat, P. V. *J. Phys. Chem. Lett.* **2012,** *3*, 1453. doi: 10.1021/jz3004206

(72) Zhang, N.; Yang, M. Q.; Liu, S.; Sun, Y.; Xu, Y. J. *Chem. Rev.* **2015,** *115*, 10307. doi: 10.1021/acs.chemrev.5b00267

(73) Tu, W.; Zhou, Y.; Liu, Q.; Tian, Z.; Gao, J.; Chen, X.; Zhang, H.; Liu, J.; Zou, Z. *Adv. Funct. Mater.* **2012,** *22*, 1215. doi: 10.1002/adfm.201102566

(74) Han, C.; Chen, Z.; Zhang, N.; Colmenares, J. C.; Xu, Y. J. *Adv. Funct. Mater.* **2015,** *25*, 221. doi: 10.1002/adfm.201402443

(75) Gao, E.; Wang, W.; Shang, M.; Xu, J. *Phys. Chem. Chem. Phys.* **2011,** *13*, 2887. doi: 10.1039/C0CP01749C

(76) Wang, P. Q.; Bai, Y.; Luo, P. Y.; Liu, J. Y. *Catal. Commun.* **2013,** *38*, 82. doi: 10.1016/j.catcom.2013.04.020

(77) Cheng, J.; Zhang, M.; Wu, G.; Wang, X.; Zhou, J.; Cen, K. *Environ. Sci. Technol.* **2014,** *48*, 7076. doi: 10.1021/es500364g

(78) Yang, K. D.; Ha, Y.; Sim, U.; An, J.; Lee, C. W.; Jin, K.; Kim, Y.; Park, J.; Hong, J. S.; Lee, J. H.; Lee, H. E.; Jeong, H. Y.; Kim, H.; Nam, K. T. *Adv. Funct. Mater.* **2016,** *26*, 233. doi: 10.1002/adfm.201502751

(79) 79) Xiao, F. X.; Pagliaro, M.; Xu, Y. J.; Liu, B. *Chem. Soc. Rev.* **2016,** (*45*, 3088. doi: 10.1039/C5CS00781J

(80) Li, Z.; Luo, W.; Zhang, M.; Feng, J.; Zou, Z. *Energy Environ. Sci.* **2013,** *6*, 347. doi: 10.1039/C2EE22618A

(81) Kecenovic, E.; Endrődi, B.; Pápa, Z.; Hernadi, K.; Rajeshwar, K.; Janaky, C. *J. Mater. Chem. A* **2016,** *4*, 3139. doi: 10.1039/C5TA10457B

(82) Shen, Q.; Chen, Z.; Huang, X.; Liu, M.; Zhao, G. *Environ. Sci. Technol.* **2015,** *49*, 5828. doi: 10.1021/acs.est.5b00066

(83) Kim, K. S.; Zhao, Y.; Jang, H.; Lee, S. Y.; Kim, J. M.; Kim, K. S.; Ahn, J. H.; Kim, P.; Choi, J. Y.; Hong, B. H. *Nature* **2009,** *457*, 706. doi: 10.1038/nature07719

(84) Juang, Z. Y.; Wu, C. Y.; Lu, A. Y.; Su, C. Y.; Leou, K. C.; Chen, F. R.; Tsai, C. H. *Carbon* **2010,** *48*, 3169. doi: 10.1016/j.carbon.2010.05.001

(85) Huang, X.; Qi, X.; Boey, F.; Zhang, H. *Chem. Soc. Rev.* **2012,** *41*, 666. doi: 10.1039/C1CS15078B

(86) Xu, C.; Xu, B.; Gu, Y.; Xiong, Z.; Sun, J.; Zhao, X. S. *Energy Environ. Sci.* **2013,** *6*, 1388. doi: 10.1039/C3EE23870A

(87) Chen, J.; Shi, J.; Wang, X.; Cui, H.; Fu, M. *Chin. J. Catal.* **2013,** *34*, 621. doi: 10.1016/S1872-2067(12)60530-0

(88) Xiang, Q.; Yu, J.; Jaroniec, M. *Chem. Soc. Rev.* **2012,** *41*, 782. doi: 10.1039/C1CS15172J

(89) Ng, Y. H.; Iwase, A.; Kudo, A.; Amal, R. *J. Phys. Chem. Lett.* **2010,** *1*, 2607. doi: 10.1021/jz100978u

(90) Sun, L.; Bai, Y.; Zhang, N.; Sun, K. *Chem. Commun.* **2015,** *51*, 1846. doi: 10.1039/C4CC08288E

(91) Li, H.; Pang, S.; Wu, S.; Feng, X.; Müllen, K.; Bubeck, C. *J. Am. Chem. Soc.* **2011,** *133*, 9423. doi: 10.1021/ja201594k

(92) Eda, G.; Emrah Unalan, H.; Rupesinghe, N.; Amaratunga, G. A. J.; Chhowalla, M. *Appl. Phys. Lett.* **2008,** *93*, 233502. doi: 10.1063/1.3028339

(93) Annamalai, A.; Kannan, A. G.; Lee, S. Y.; Kim, D. W.; Choi, S. H.; Jang, J. S. *J. Phys. Chem. C* **2015,** *119*, 19996. doi: 10.1021/acs.jpcc.5b06450

(94) Chen, Z.; Ren, W.; Gao, L.; Liu, B.; Pei, S.; Cheng, H. M. *Nat. Mater.* **2011,** *10*, 424. doi: 10.1038/nmat3001

(95) Li, X.; Cai, W.; An, J.; Kim, S.; Nah, J.; Yang, D.; Piner, R.; Velamakanni, A.; Jung, I.; Tutuc, E.; Banerjee, S. K.; Colombo,

L.; Ruoff, R. S. *Science* **2009,** *324*, 1312. doi: 10.1126/science.1171245

(96) Yu, C.; Meng, X.; Song, X.; Liang, S.; Dong, Q.; Wang, G.; Hao, C.; Yang, X.; Ma, T.; Ajayan, P. M.; Qiu, J. *Carbon* **2016,** *100*, 474. doi: 10.1016/j.carbon.2016.01.042

(97) Shin, S.; Kim, S.; Kim, T.; Du, H.; Kim, K. S.; Cho, S.; Seo, S. *Carbon* **2017,** *111*, 215. doi: 10.1016/j.carbon.2016.09.077

(98) Gao, L.; Ren, W.; Xu, H.; Jin, L.; Wang, Z.; Ma, T.; Ma, L. P.; Zhang, Z.; Fu, Q.; Peng, L. M.; Bao, X.; Cheng, H. M. *Nat. Commun.* **2012,** *3*, 699. doi: 10.1038/ncomms1702

(99) Wang, H.; Yu, G. *Adv. Mater.* **2016,** *28*, 4956. doi: 10.1002/adma.201505123

(100) Teng, P. Y.; Lu, C. C.; Akiyama-Hasegawa, K.; Lin, Y. C.; Yeh, C. H.; Suenaga, K.; Chiu, P. W. *Nano Lett.* **2012,** *12*, 1379. doi: 10.1021/nl204024k

(101) Wei, D.; Lu, Y.; Han, C.; Niu, T.; Chen, W.; Wee, A. T. *Angew. Chem. Int. Ed.* **2013,** *52*, 14121. doi: 10.1002/anie.201306086

(102) Yang, W.; Chen, G.; Shi, Z.; Liu, C. C.; Zhang, L.; Xie, G.; Cheng, M.; Wang, D.; Yang, R.; Shi, D.; Watanabe, K.; Taniguchi, T.; Yao, Y.; Zhang, Y.; Zhang, G. *Nat. Mater.* **2013,** *12*, 792. doi: 10.1038/nmat3695

(103) Yuan, Y. P.; Ruan, L. W.; Barber, J.; Joachim Loo, S. C.; Xue, C. *Energy Environ. Sci.* **2014,** *7*, 3934. doi: 10.1039/C4EE02914C

(104) An, S. J.; Zhu, Y.; Lee, S. H.; Stoller, M. D.; Emilsson, T.; Park, S.; Velamakanni, A.; An, J.; Ruoff, R. S. *J. Phys. Chem. Lett.* **2010,** *1*, 1259. doi: 10.1021/jz100080c

(105) Yang, Y.; Li, J.; Chen, D.; Zhao, J. *ACS Appl. Mater. Interfaces* **2016,** *8*, 26730. doi: 10.1021/acsami.6b07990

(106) Chen, L.; Tang, Y.; Wang, K.; Liu, C.; Luo, S. *Electrochem. Commun.* **2011,** *13*, 133. doi: 10.1016/j.elecom.2010.11.033

(107) Li, F.; Zhang, L.; Tong, J.; Liu, Y.; Xu, S.; Cao, Y.; Cao, S. *Nano Energy 27*, 320. doi: 10.1016/j.nanoen.2016.06.056

(108) Liu, C.; Teng, Y.; Liu, R.; Luo, S.; Tang, Y.; Chen, L.; Cai, Q. *Carbon* **2011,** *49*, 5312. doi: 10.1016/j.carbon.2011.07.051

(109) Liu, C.; Wang, K.; Luo, S.; Tang, Y.; Chen, L. *Small* **2011,** *7*, 1203. doi: 10.1002/smll.201002340

(110) Tang, J.; Zhang, Y.; Kong, B.; Wang, Y.; Da, P.; Li, J.; Elzatahry, A. A.; Zhao, D.; Gong, X.; Zheng, G. *Nano Lett.* **2014,** *14*, 2702. doi: 10.1021/nl500608w

(111) Bessegato, G. G.; Guaraldo, T. T.; Brito, J. F.; Brugnera, M. F.; Zanoni, M. V. B. *Electrocatalysis* **2015,** *6*, 415. doi: 10.1007/s12678-015-0259-9

(112) Zhang, M.; Cheng, J.; Xuan, X.; Zhou, J.; Cen, K. *ACS Sustainable Chem. Eng.* **2016,** *4*, 6344. doi: 10.1021/acssuschemeng.6b00909

(113) Cheng, J.; Zhang, M.; Wu, G.; Wang, X.; Zhou, J.; Cen, K. *Sol. Energy Mater. Sol. Cells* **2015,** *132*, 606. doi: 10.1016/j.solmat.2014.10.015

(114) Pathak, P.; Gupta, S.; Grosulak, K.; Imahori, H.; Subramanian, V. *J. Phys. Chem. C* **2015,** *119*, 7543. doi: 10.1021/jp512160h

(115) Ng, Y. H.; Lightcap, I. V.; Goodwin, K.; Matsumura, M.; Kamat, P. V. *J. Phys. Chem. Lett.* **2010,** *1*, 2222. doi: 10.1021/jz100728z

(116) Lightcap, I. V.; Kamat, P. V. *J. Am. Chem. Soc.* **2012,** *134*, 7109. doi: 10.1021/ja3012929

(117) Hasan, M. R.; Abd Hamid, S. B.; Basirun, W. J.; Meriam Suhaimy, S. H.; Che Mat, A. N. *RSC Adv.* **2015,** *5*, 77803. doi: 10.1039/C5RA12525A

(118) Liang, Y.; Li, Y.; Wang, H.; Zhou, J.; Wang, J.; Regier, T.; Dai, H. *Nat. Mater.* **2011,** *10*, 780. doi: 10.1038/nmat3087

(119) Wu, Z. S.; Yang, S.; Sun, Y.; Parvez, K.; Feng, X.; Müllen, K. *J. Am. Chem. Soc.* **2012,** *134*, 9082. doi: 10.1021/ja3030565

(120) Huang, X.; Cao, T.; Liu, M.; Zhao, G. *J. Phys. Chem. C* **2013,** *117*, 26432. doi: 10.1021/jp408630s

(121) Sekizawa, K.; Maeda, K.; Domen, K.; Koike, K.; Ishitani, O. *J. Am. Chem. Soc.* **2013,** *135*, 4596. doi: 10.1021/ja311541a

(122) Jin, J.; Yu, J.; Guo, D.; Cui, C.; Ho, W. *Small* **2015,** *11*, 5262. doi: 10.1002/smll.201500926

(123) Iwashina, K.; Iwase, A.; Ng, Y. H.; Amal, R.; Kudo, A. *J. Am. Chem. Soc.* **2015,** *137*, 604. doi: 10.1021/ja511615s

(124) Xian, J.; Li, D.; Chen, J.; Li, X.; He, M.; Shao, Y.; Yu, L.; Fang, J. *ACS Appl. Mater. Interfaces* **2014,** *6*, 13157. doi: 10.1021/am5029999

(125) Li, P.; Zhou, Y.; Li, H.; Xu, Q.; Meng, X.; Wang, X.; Xiao, M.; Zou, Z. *Chem. Commun.* **2015,** *51*, 800. doi: 10.1039/C4CC08744E

(126) Maeda, K. *ACS Catal.* **2013,** *3*, 1486. doi: 10.1021/cs4002089

(127) Zhou, P.; Yu, J.; Jaroniec, M. *Adv. Mater.* **2014,** *26*, 4920. doi: 10.1002/adma.201400288

(128) Arai, T.; Sato, S.; Kajino, T.; Morikawa, T. *Energy Environ. Sci.* **2013,** *6*, 1274. doi: 10.1039/C3EE24317F

(129) Arai, T.; Sato, S.; Uemura, K.; Morikawa, T.; Kajino, T.; Motohiro, T. *Chem. Commun.* **2010,** *46*, 6944. doi: 10.1039/C0CC02061C

(130) Iwase, A.; Yoshino, S.; Takayama, T.; Ng, Y. H.; Amal, R.; Kudo, A. *J. Am. Chem. Soc.* **2016,** *138*, 10260. doi: 10.1021/jacs.6b05304

(131) Kondratenko, E. V.; Mul, G.; Baltrusaitis, J.; Larrazabal, G. O.; Perez-Ramirez, J. *Energy Environ. Sci.* **2013,** *6*, 3112. doi: 10.1039/C3EE41272E

(132) Christensen, P. A.; Curtis, T. P.; Egerton, T. A.; Kosa, S. A. M.; Tinlin, J. R. *Appl. Catal., B* **2003,** *41*, 371. doi: 10.1016/s0926-3373(02)00172-8

(133) Gangeri, M.; Perathoner, S.; Caudo, S.; Centi, G.; Amadou, J.; Bégin, D.; Pham-Huu, C.; Ledoux, M. J.; Tessonnier, J. P.; Su, D. S.; Schlögl, R. *Catal. Today* **2009,** *143*, 57. doi: 10.1016/j.cattod.2008.11.00